

Figure 3.5.1: Quantum-perturbative plot for 3-level model of with arbitrary (non-physical) parameters. Red plot is for the imaginary and the blue plot is for the real part of the linear susceptibility.

4 Simpson and trapezoidal quadrature based Hilbert transform - HTRAN

4.1 Overview of the HTRAN

In this chapter we present the simplest possible ~~x~~ but still nice working numerical calculation of the Hilbert transform ~~x~~ based on the report by I. J. Weinberg [45]. It uses the Simpson and trapezoidal quadrature. We have slightly modified author's algorithm and it no longer requires the input to be an even function.

The algorithm is presented in two parts. In the first part, we present how the Hilbert transform equation can be modified with one strict assumption from the singular integral to the typical non-singular ~~one~~ quadrature. In the second part, we will use the new set of input function values based on the interpolation method.

We assume that the input function R is defined for a discrete set of arguments:

$$F = \{F_1, F_2, \dots, F_N\} \quad (\text{for } F_i < F_j \text{ for } i < j). \quad (4.1.1)$$

We will calculate the Hilbert transform of R for the same discrete set of arguments F . An example has been presented on the Figure (4.1.1), where the blue plot represents the input function R and the green plot represents the output function HT .

We start from the modification of the main Hilbert transform equation from the basic representation (second term) into a limit of two integrals (third term):

$$\text{HT}(\omega) = \frac{1}{\pi} \int_{-\infty}^{\infty} \frac{R(\Omega)}{\Omega - \omega} d\Omega = \lim_{\epsilon \rightarrow 0} \left(\int_{-\infty}^{\omega - \epsilon} \frac{R(\Omega)}{\Omega - \omega} d\Omega + \int_{\omega + \epsilon}^{\infty} \frac{R(\Omega)}{\Omega - \omega} d\Omega \right). \quad (4.1.2)$$

Now for each frequency ω we observe the following property:

$$\int_{-\infty}^{\infty} \frac{1}{\Omega - \omega} d\Omega = 0. \quad (4.1.3)$$

We use the observation (4.1.3) and modify the equation (4.1.2):

We start from reminding the definition of the Hilbert transform:

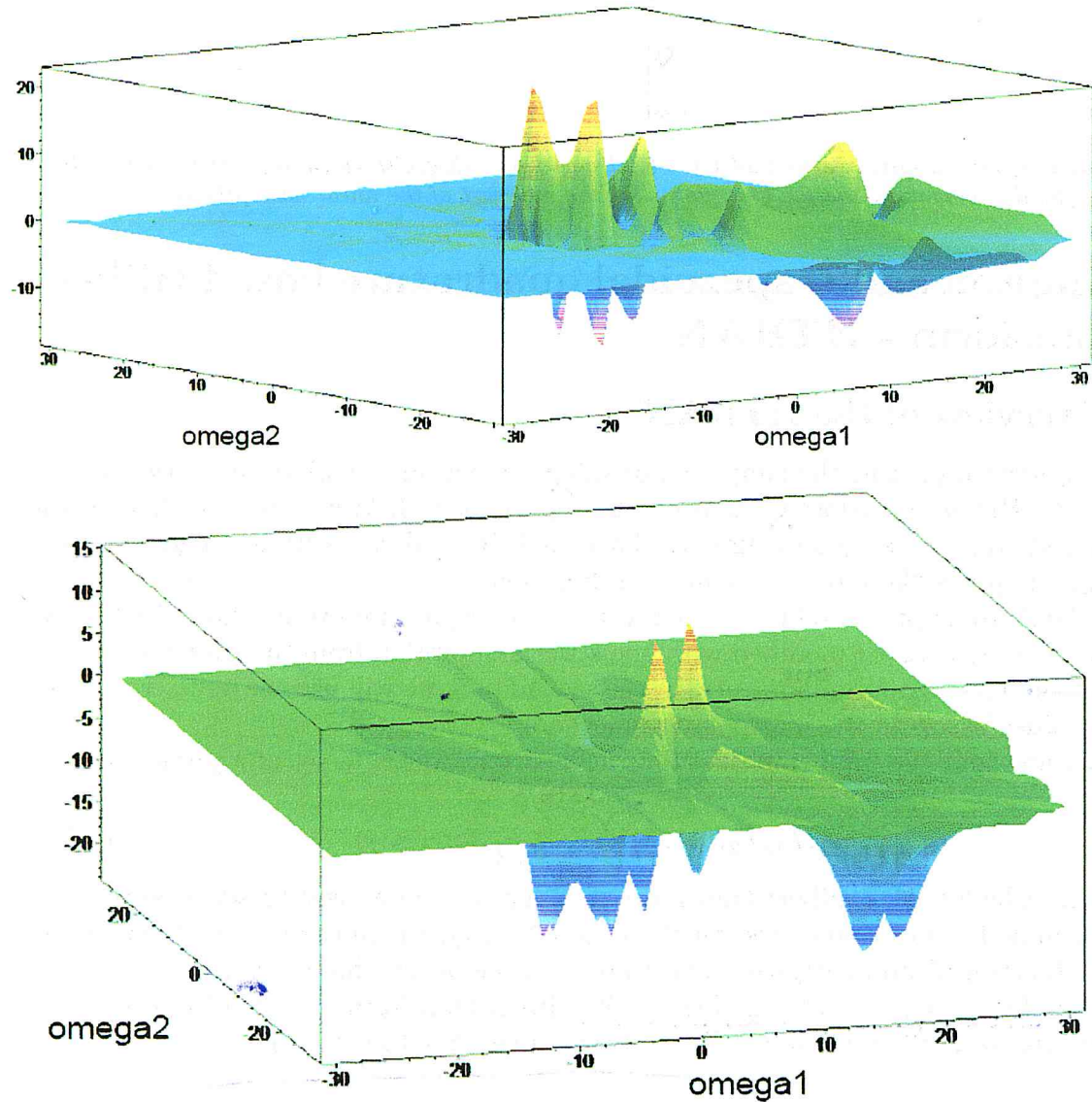


Figure 3.5.2: Quantum-perturbative plot for 3-level model of with arbitrary (non-physical) parameters. Red plot is for the imaginary and the blue plot is for the real part of the second-order susceptibility.

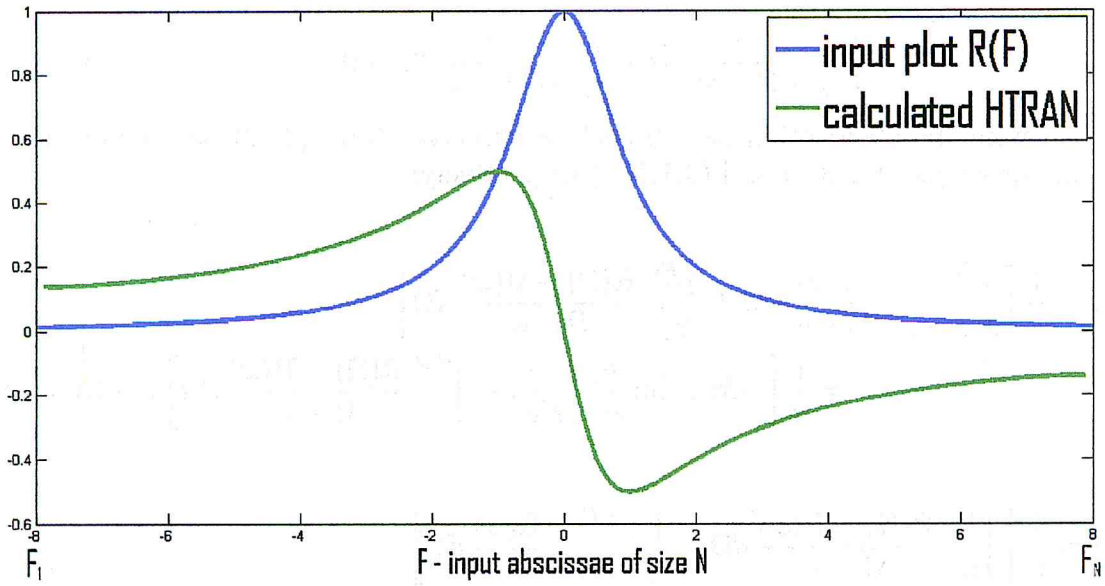


Figure 4.1.1: A sample input plot (ordered pairs of OX abscissae - F - and the OY ordinates - R) with the sample output plot HT for the HTRAN algorithm.

$$HT(\omega) = \frac{1}{\pi} \int_{-\infty}^{\infty} \frac{R(\Omega) - R(\omega)}{\Omega - \omega} d\Omega + \frac{1}{\pi} \int_{-\infty}^{\infty} \frac{R(\Omega)}{\Omega - \omega} d\Omega = \frac{1}{\pi} \int_{-\infty}^{\infty} \frac{R(\Omega) - R(\omega)}{\Omega - \omega} d\Omega. \quad (4.1.4)$$

We can easily transform the result of the (4.1.4) as follows:

$$HT(\omega) = \frac{1}{\pi} \left[\int_{-\infty}^{F_1} \frac{R(\Omega) - R(\omega)}{\Omega - \omega} d\Omega + \int_{F_1}^{F_N} \frac{R(\Omega) - R(\omega)}{\Omega - \omega} d\Omega + \int_{F_N}^{\infty} \frac{R(\Omega) - R(\omega)}{\Omega - \omega} d\Omega \right]. \quad (4.1.5)$$

As the input R function is assumed to be square-integrable, we will put even more strict assumption:

$$R(\omega) = 0 \text{ for } \omega < F_1 \text{ or } \omega > F_N. \quad (4.1.6)$$

With the strict-vanishing assumption (4.1.6) for $R(\omega)$, we can simplify the equation (4.1.5) as follows:

$$HT(\omega) = \frac{1}{\pi} \left[\int_{-\infty}^{F_1} -\frac{R(\omega)}{\Omega - \omega} d\Omega + \int_{F_1}^{F_N} \frac{R(\Omega) - R(\omega)}{\Omega - \omega} d\Omega + \int_{F_N}^{\infty} -\frac{R(\omega)}{\Omega - \omega} d\Omega \right]. \quad (4.1.7)$$

As $\omega \in [F_1, F_N]$ we will now consider two cases - that takes into account the position of ω in relation to F_1 and F_N . We have two possibilities:

$$\omega - F_1 < F_N - \omega \text{ and } F_N - \omega \leq \omega - F_1 \quad (4.1.8)$$

We shall also notice the symmetry property of the function $\frac{1}{\Omega - \omega}$ for any $M > 0$:

$$\int_{-\infty}^{\omega-M} \frac{1}{\Omega - \omega} d\Omega + \int_{\omega+M}^{\infty} \frac{1}{\Omega - \omega} d\Omega = 0 \quad (4.1.9)$$

Together with the observation (4.1.9) each of two cases from (4.1.8) leads to results obtained in equations (4.1.10a) and (4.1.10b) respectively:

$$\begin{aligned} \text{HT}(\omega) &= \frac{1}{\pi} \left[\int_{2\omega-F_N}^{F_1} -\frac{R(\omega)}{\Omega - \omega} d\Omega + \int_{F_1}^{F_N} \frac{R(\Omega) - R(\omega)}{\Omega - \omega} d\Omega \right] \\ &= \frac{1}{\pi} \left[-R(\omega) \ln\left(\frac{F_1 - \omega}{\omega - F_N}\right) + \int_{F_1}^{F_N} \frac{R(\Omega) - R(\omega)}{\Omega - \omega} d\Omega \right], \end{aligned} \quad (4.1.10a)$$

$$\begin{aligned} \text{HT}(\omega) &= \frac{1}{\pi} \left[\int_{F_1}^{F_N} \frac{R(\Omega) - R(\omega)}{\Omega - \omega} d\Omega + \int_{F_N}^{2\omega-F_1} \frac{-R(\omega)}{\Omega - \omega} d\Omega \right] \\ &= \frac{1}{\pi} \left[\int_{F_1}^{F_N} \frac{R(\Omega) - R(\omega)}{\Omega - \omega} d\Omega - R(\omega) \ln\left(\frac{\omega - F_1}{F_N - \omega}\right) \right]. \end{aligned} \quad (4.1.10b)$$

And we can see that both the 4.1.10 derivations lead to the same result:

$$\text{HT}(\omega) = \frac{1}{\pi} \left[-R(\omega) \ln\left(\frac{\omega - F_1}{F_N - \omega}\right) + \int_{F_1}^{F_N} \frac{R(\Omega) - R(\omega)}{\Omega - \omega} d\Omega \right] \quad (4.1.11)$$

We also observe that for any ω inside the range $[F_1, F_N]$ both values $\omega - F_1$ and $F_N - \omega$ are non-negative. That leads to a simple observation that condition $0 < \frac{\omega - F_1}{F_N - \omega}$ is satisfied and therefore the logarithm argument is well defined. What now interests us the most, is the integral:

$$Y(\omega) = \int_{F_1}^{F_N} \frac{R(\Omega) - R(\omega)}{\Omega - \omega} d\Omega \quad (4.1.12)$$

We would like the denominator in the (4.1.12) equation never equals zero, so we can calculate the whole integral numerically. For this reason we are preparing a new set of values, which are just a simple midways of F :

$$\widehat{F}_k = \frac{F_k + F_{k+1}}{2} \quad \text{for } k = 1 \dots N-1 \quad \text{check!} \quad (4.1.13)$$

We will also need to approximate the values of a new \widehat{R} at $\widehat{F}_j (j = 1 \dots N-1)$ values. We will do this by a simple cubic interpolation:

$$\underline{R(\widehat{F}_1)} = \widehat{R}_1 = \frac{3R_1 + 6R_2 - R_3}{8} \quad (4.1.14a)$$

$$\widehat{R}_k = \frac{-R_{k-1} + 9R_k + 9R_{k+1} - R_{k+2}}{16} \quad \text{check!} \quad \text{for } k = 2 \dots N-2 \quad (4.1.14b)$$

$$\widehat{R}_{N-1} = \frac{-R_{N-2} + 6R_{N-1} + 3R_N}{8} \quad (4.1.14c)$$

By now, the calculation of the Y function from the (4.1.12) equation will be performed by a simple quadrature integration. The introduced \widehat{Y}_i symbol describes the numerical approximation of the Y function calculated with the following equation:

$$\widehat{Y}_i = \sum_{j=1}^N \frac{h_j (R_j - \widehat{R}_i)}{F_j - \widehat{F}_i} \text{ for } i = 1 \dots N-1. \quad (4.1.15)$$

To do such an integration we will hire the Simpson's rule. If N is odd, we have:

$$h_1 = h_N = \frac{F_2 - F_1}{3} = \frac{\Delta F}{3} \quad (4.1.16a)$$

$$h_j = \frac{4 \Delta F}{3} \text{ for } j = 2, 4 \dots N-1 \quad (4.1.16b)$$

$$h_j = \frac{2 \Delta F}{3} \text{ for } j = 3, 5 \dots N-2 \quad (4.1.16c)$$

If N is even, the last interval should be obtained using the trapezoidal rule:

$$h_1 = \frac{\Delta F}{3} = \frac{F_2 - F_1}{3} \quad (4.1.17a)$$

$$h_j = \frac{4 \Delta F}{3} \text{ for } j = 2, 4 \dots N-2 \quad (4.1.17b)$$

$$h_j = \frac{2 \Delta F}{3} \text{ for } j = 3, 5 \dots N-3 \quad (4.1.17c)$$

$$h_{N-1} = \frac{5 \Delta F}{6} \quad (4.1.17d)$$

$$h_N = \frac{\Delta F}{2} \quad (4.1.17e)$$

In the next step, we calculate the Hilbert transform at points $\widehat{F}_j (j = 1, \dots, N-1)$:

$$\widehat{HT}_i = \frac{1}{\pi} \left[-\widehat{R}_i \ln \left(\frac{\widehat{F}_i - F_1}{F_N - \widehat{F}_i} \right) + \widehat{Y}_i \right]. \quad (4.1.18)$$

Finally we need to undo the cubic interpolation. To do so, we perform the following calculations:

$\checkmark HF(F_1) = HT_1, \text{ qdr c : } \checkmark$

$$HF(F_1) = HT_1 = \frac{15 \widehat{HT}_1 - 10 \widehat{HT}_2 + 3 \widehat{HT}_3}{8} \quad (4.1.19a)$$

$$HT_2 = \frac{3 \widehat{HT}_1 + 6 \widehat{HT}_2 - 1 \widehat{HT}_3}{8} \quad (4.1.19b)$$

$$HT_i = \frac{-\widehat{HT}_{i-1} + 9 \widehat{HT}_i + 9 \widehat{HT}_{i+1} - \widehat{HT}_{i+2}}{16} \text{ for } i = 3, 4, \dots, N-2 \quad (4.1.19c)$$

$$HT_{N-1} = \frac{-\widehat{HT}_{N-3} + 6 \widehat{HT}_{N-2} + 3 \widehat{HT}_{N-1}}{8} \quad (4.1.19d)$$

$$HT_N = \frac{3 \widehat{HT}_{N-3} - 10 \widehat{HT}_{N-2} + 15 \widehat{HT}_{N-1}}{8} \quad (4.1.19e)$$

In following chapters we will show the results obtained with this method.

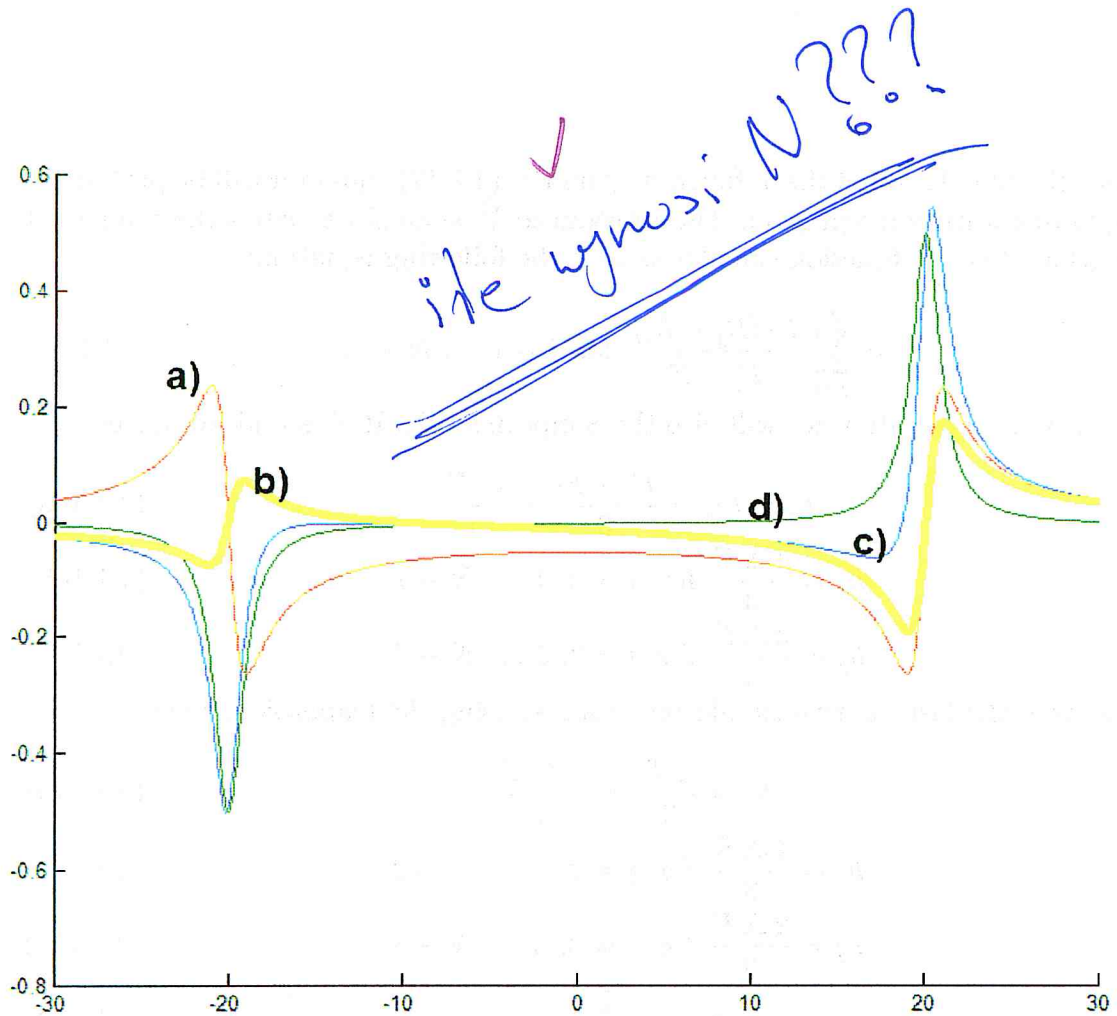


Figure 4.2.1: The Figure presents the results of the HTRAN method applied for the simple linear model. Results are plotted together a) The plot of the real part of $\chi(\omega)$ b) absolute error plot (c-plot minus d-plot) c) imaginary part of $\chi(\omega)$ obtained with the Hilbert transform of a-plot d) part of $\chi(\omega)$ [im] calculated analytically.

4.2 HTRAN for simple linear model - results

We shall remind the model presented in Chapter (3) in the equation 3.3.3

$$\mathcal{F}[h_{\text{lin}}] = \chi_{\text{lin}}(\omega) \approx \frac{-20}{(\omega i + 1 - 20i)(\omega i + 1 + 20i)}. \quad (4.2.1)$$

The real part of χ_{lin} will be used as the input R function in the equation (4.1.2). The output HT function calculated with the HTRAN algorithm is compared to the imaginary part of the χ_{lin} . We have presented the results in the Figure 4.2.1. In this and in the following chapters we would like the error function represented with the yellow colour to be as close to zero as possible. We also would like the numerical results to be close to the values calculated analytically.

4.3 HTRAN for simple nonlinear model - results

We remind the equation for the pump-and-probe susceptibility model (3.4.1):

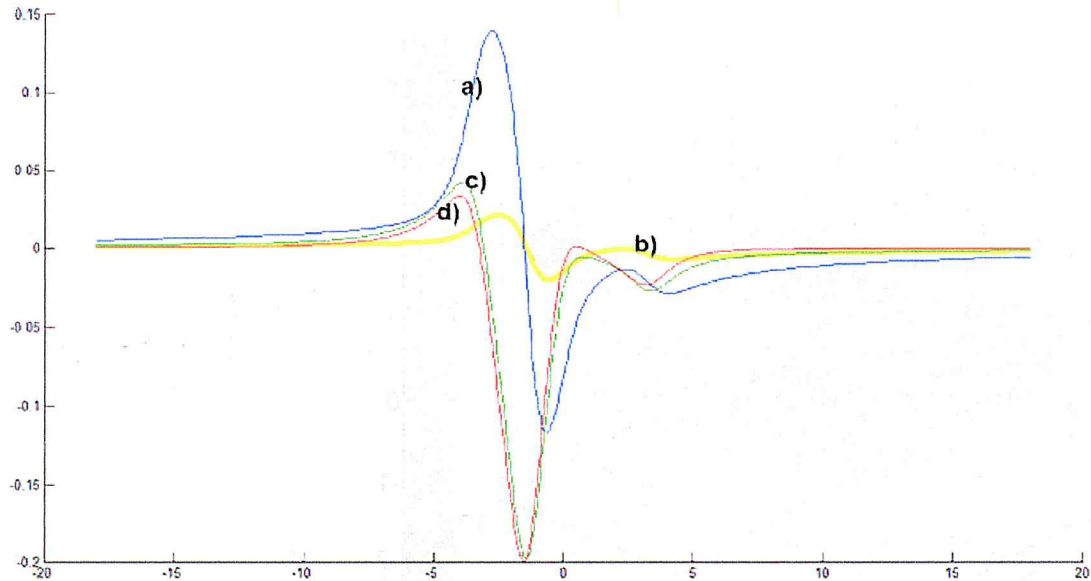


Figure 4.3.1: The Figure presents the results of the HTRAN method applied for the pump-and-probe model. Results are plotted together a) The plot of the real part of $\chi_{pp}(\omega)$ b) absolute error plot (c-plot minus d-plot) c) imaginary part of $\chi_{pp}(\omega)$ d) imaginary part of $\chi_{pp}(\omega)$ calculated analytically.

$$\chi_{pp}(\delta) = \frac{G n_0 \gamma_{ba}}{\Delta + \delta + I\eta} \left(1 - \frac{\Omega_1^2 (\Delta - \delta + I\eta)(\delta + 2I\eta)}{(\Delta - I\eta)((\delta + I\theta)(\Delta + \delta + I\eta)(\delta - \Delta + I\eta) - \Omega_1^2(\delta + I\eta))^2} \right) \quad (4.3.1)$$

$$G = 1,$$

$$\gamma_{ba} = 1,$$

$$n_0 = 1,$$

$$\Delta = 1.3,$$

$$\eta = 1,$$

$$\theta = 1.4,$$

$$\Omega_1 = 4.3.$$

and we have assigned the values for the constants:

The results for such set of arbitrary parameters are shown on the Figure 4.3.1.

The resulted b-plot seems to be a not-so-bad introduction into the Hilbert transform evaluation, as we have only employed the simple Simpson's rule. We would also like to perform the three-dimensional analysis of the assumed pump-probe susceptibility, so we employ the (3.4.9a) and (3.4.9b) equations for each frequency, which require performing two integrations (one for each frequency-domain argument). Unfortunately, only the obtained three-dimensional shapes are similar to the original ones, but we have received a huge relative error as presented in the Figure 4.3.2.

Let's now perform the evaluation for the wave-mixing model as stated in the model described by (3.4.5a). We expand this equation to resolve the complex conjugate of D function and the resulting function is:

LET'S REVIEW THE
HWM model (3.4.5a) stated
in (3.4.5a):

GO TO D?

Review
(3.4.5a)

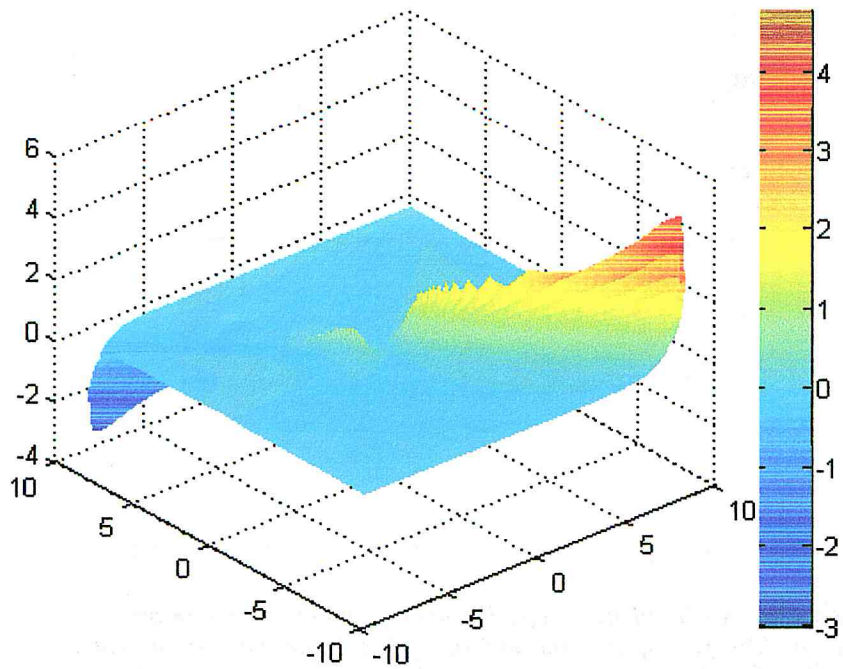


Figure 4.3.2: The Figure presents the combined relative error for the results of the HTRAN method applied for the two-dimensional pump-and-probe model. The light-cyan colour shows the area of error below 100%. \checkmark

$$\chi_{mix}(\delta) = \frac{2 N w_0 \mu_{ba}^4}{3 \epsilon_0 h^3} (-\delta - \Delta - \frac{i}{T_2}) (\delta + \frac{2i}{T_2}) ((\Delta + \frac{i}{T_2}) (\Delta + \delta + \frac{i}{T_2})) \quad (4.3.2)$$

$$(\delta^3 - \frac{2i\delta^2}{T_2} - \delta\Delta^2 - \frac{2i\delta}{T_1 T_2} - \frac{\delta}{T_2^2} + \frac{\delta^2}{T_1} - \frac{\Delta^2}{T_1} - \frac{1}{T_1 T_2^2} - \Omega_2 \delta + \frac{\Omega_2 i}{T_2}))$$

With such a complex function we obtain the following two and three dimensional results on Figure (4.3.3). \checkmark

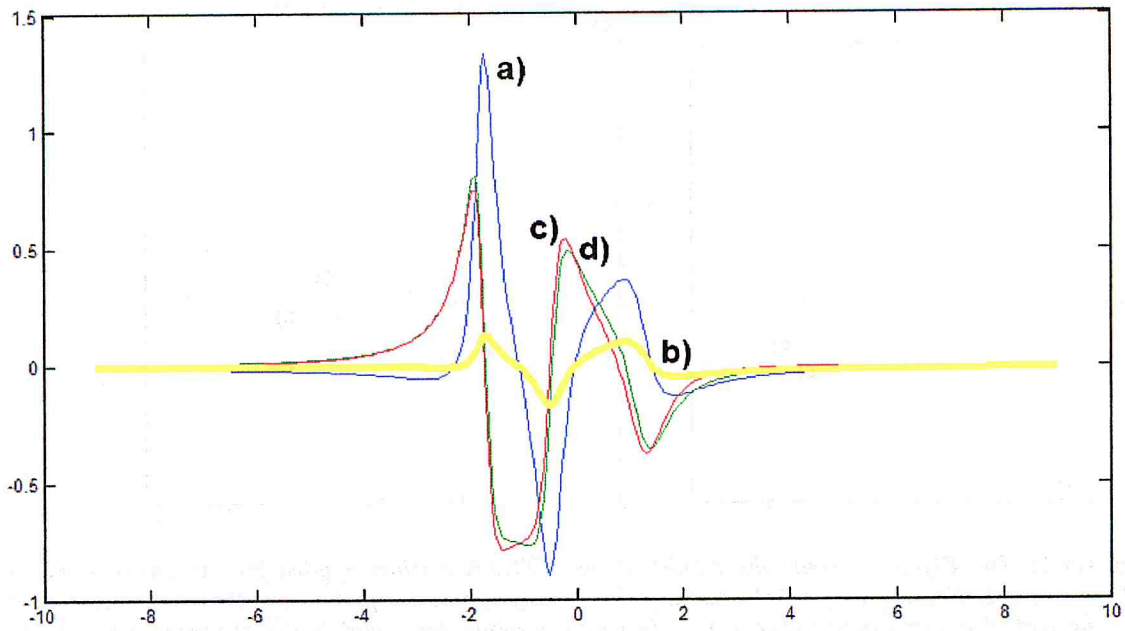
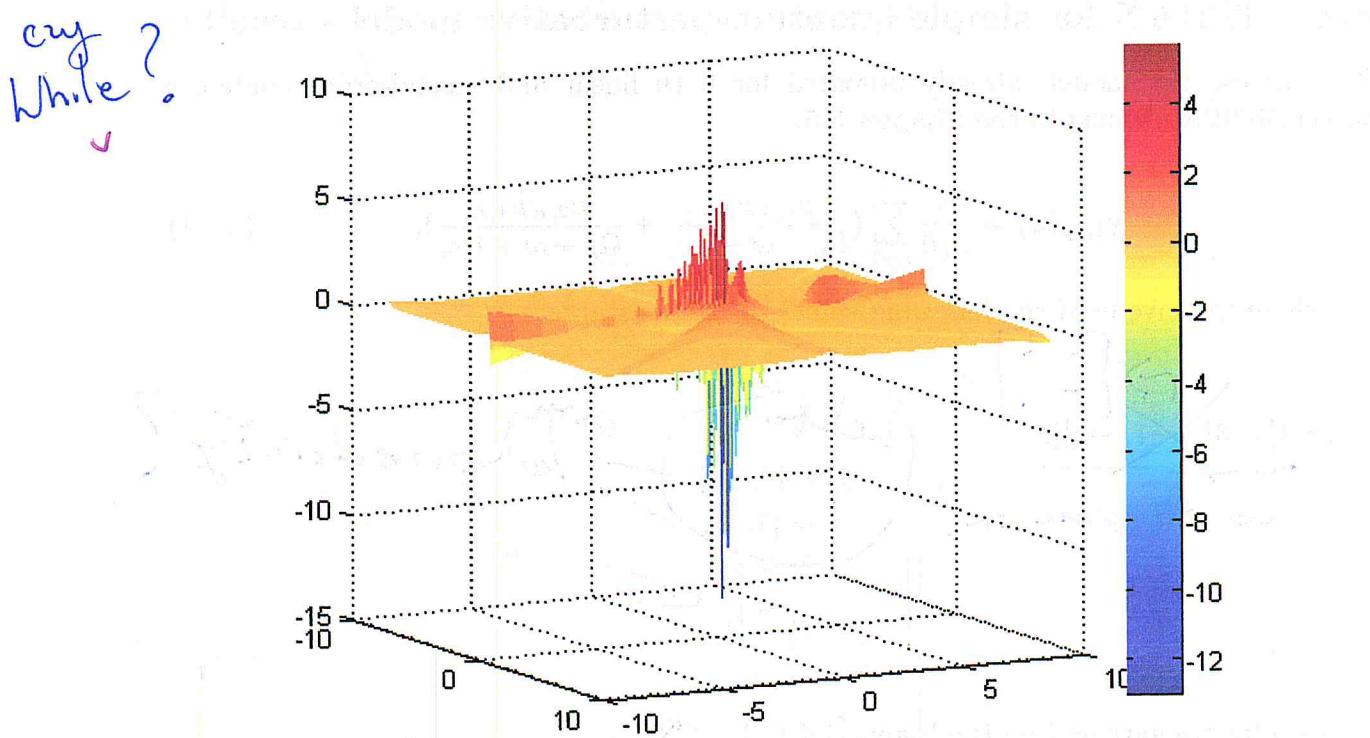


Figure 4.3.3: The Figure presents the combined relative error for the results of the HTRAN method applied for the two-dimensional wave-mixing model. a) The plot of the real part of $\chi_{mix}(\omega)$ b) absolute error plot (c-plot minus d-plot) c) (red) imaginary part of $\chi_{mix}(\omega)$ d) (grey) imaginary part of $\chi_{mix}(\omega)$ calculated analytically.

As the obtained three-dimensional shape looks very similar to those obtained analytically, the relative error still remains huge for some areas (Figure 4.3.4):



podj. > my solution

↙

Julie billy sa ova u your
v vite... v (to pytanie do fizyku) \otimes

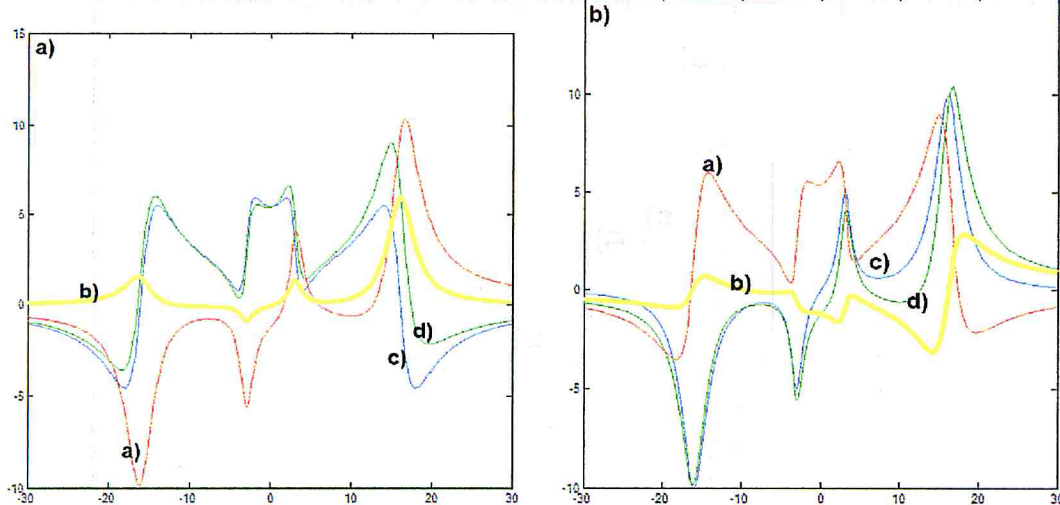


Figure 4.4.1: The Figure presents the results of the HTRAN method applied for the linear quantum-perturbative model. The results for both real and imaginary values are plotted together on Figures a and b: a.a) The plot of the imaginary part of $\chi_{1,qp}(\omega)$ a.b) absolute error plot (a.d-plot minus a.c-plot) a.c) real part of $\chi_{1,qp}(\omega)$ calculated analytically a.d) real part of $\chi_{1,qp}(\omega)$ obtained with the Hilbert transform of a-plot b.a) The plot of the real part of $\chi_{1,qp}(\omega)$ b.b) absolute error plot (b.d-plot minus b.c-plot) b.c) imaginary part of $\chi_{1,qp}(\omega)$ calculated analytically b.d) imaginary part of $\chi_{1,qp}(\omega)$ obtained with the Hilbert transform of a-plot

Figure 4.3.4: The Figure presents the combined relative error for the real part of nonlinear susceptibility $\chi_{mix}(\delta)$ describing the wave-mixing process.

4.4 HTRAN for simple quantum-perturbative model - results

We will use the models already prepared for both linear and second-order nonlinear susceptibilities defined in the Chapter 3.5.

$$\chi_{1,qp}(\omega) = \frac{N}{\epsilon_0 \hbar} \sum_{n=1}^2 \left(\frac{\mu_{1,n} \mu_{2,n}}{\Omega_n - \omega - i\gamma_n} + \frac{\mu_{2,n} \mu_{1,n}}{\Omega_n + \omega + i\gamma_n} \right), \quad (4.4.1)$$

where we have used the following values of the constants:

~~never~~ $\mu = [[1, 3], [-1, -2]]$, $\Omega = [3, 16]$, $\gamma = [1, 2]$, $N = 5$, $\epsilon_0 = 1$, $\hbar = -1$

what for omega?

over to predict?

Results are gathered on the Figure 4.4.1. \otimes

(tak, wony są symetryczne)
 czyli reciprosta nie jest równa jaka dana,
 skąd zatem tu jest ona taka wynikiem?

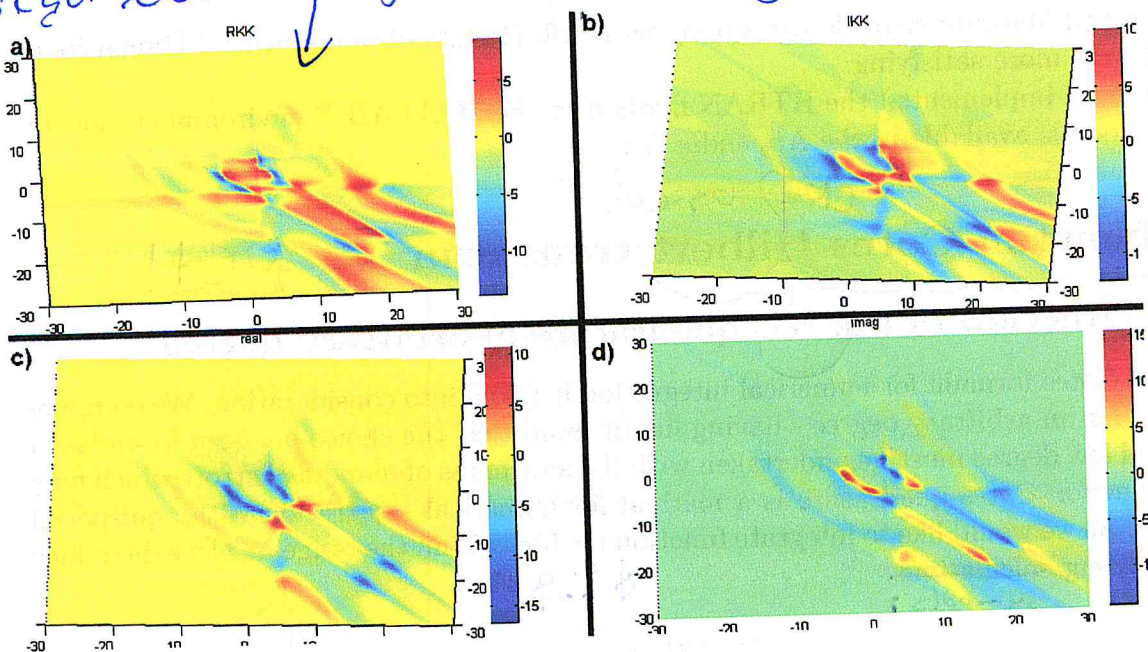


Figure 4.4.2: The Figure presents the results of the HTRAN method applied for the second-order non-linear quantum-perturbative model. Results in the three-dimensional-like plot are plotted together. a) - The calculated real part of $\chi_{2,qp}$ b) The calculated imaginary part of $\chi_{2,qp}$ c) The real part of nonlinear susceptibility $\chi_{2,qp}$ calculated analytically d) The imaginary part of the nonlinear susceptibility $\chi_{2,qp}$

$$\begin{aligned} \chi_{2,qp}(\omega_1, \omega_2) = & 2 N \varepsilon_0 h^2 \sum_{n=1}^2 \sum_{m=1}^2 \sum_{l=1}^2 \left(\frac{\mu_{l,n} \mu_{nm} \mu_{ml}}{(\Omega_{nl} - \omega_1 - \omega_2 - i \gamma_{nl})(\Omega_{ml} - \omega_1 - i \gamma_{ml})} + \right. \\ & + \frac{\mu_{l,n} \mu_{nm} \mu_{ml}}{(\Omega_{nl} - \omega_1 - \omega_1 - i \gamma_{nl})(\Omega_{ml} - \omega_2 - i \gamma_{ml})} + \\ & + \frac{\mu_{l,n} \mu_{nm} \mu_{ml}}{(\Omega_{mn} - \omega_1 - \omega_2 - i \gamma_{mn})(\Omega_{nl} + \omega_2 + i \gamma_{nl})} + \\ & + \frac{\mu_{l,n} \mu_{nm} \mu_{ml}}{(\Omega_{mn} - \omega_1 - \omega_2 - i \gamma_{mn})(\Omega_{nl} + \omega_2 + i \gamma_{nl})} + \\ & + \frac{\mu_{l,n} \mu_{nm} \mu_{ml}}{(\Omega_{nm} + \omega_1 + \omega_2 + i \gamma_{nm})(\Omega_{ml} - \omega_1 - i \gamma_{ml})} + \\ & + \frac{\mu_{l,n} \mu_{nm} \mu_{ml}}{(\Omega_{nm} + \omega_1 + \omega_2 + i \gamma_{nm})(\Omega_{ml} - \omega_1 - i \gamma_{ml})} + \\ & + \frac{\mu_{l,n} \mu_{nm} \mu_{ml}}{(\Omega_{ml} + \omega_1 + \omega_2 + i \gamma_{ml})(\Omega_{nl} + \omega_1 + i \gamma_{nl})} + \\ & \left. + \frac{\mu_{l,n} \mu_{nm} \mu_{ml}}{(\Omega_{ml} + \omega_1 + \omega_2 + i \gamma_{ml})(\Omega_{nl} + \omega_2 + i \gamma_{nl})} \right). \quad (4.4.2) \end{aligned}$$

X X
OK
? →
χ₁ χ₂
od nowa
zrozd

In the 4.4.2 we are using the following constants' values: $\mu = [[1, 3], [-1, -2]]$, $\Omega = [[3, 16], [4, 12]]$, $\gamma = [[1, 2], [-1, 3]]$, $N = 5$, $\varepsilon_0 = 1$, $h = -1$.
 In the Figure 4.4.2 we can see that there is a similarity in obtained plots, but both the

Rozbiega się oznaczenie

relative and absolute error do not satisfy us at all. Results obtained with 2-Dimensional model were more satisfying.

We have implemented the HTRAN method in the MATLAB® environment, and its source code is available in the Appendix A.1.

Newton-Cotes Hilbert transform - NCH

5.1 Overview of the NC quadrature of arbitrary degree

Newton-Cotes formula for numerical integration is taken into consideration. We compare formula for an arbitrary degree - having in our mind that the choice between formulas of high and low degree must be undertaken with the awareness of numerical errors which may arise. Newton-Cotes quadrature is a method for numerical integration with equispaced vertices. As we would like to integrate function $f = f(x)$ within the range $[a, b]$ we introduce the following calculations.

symbols:

$$x_{n,k} = a + \frac{(b-a)}{n} k \text{ for } k = 0, 1, \dots, n \quad (5.1.1a)$$

$$\omega_n(x) = (x - x_{n,0})(x - x_{n,1}), \dots, (x - x_{n,n}) \quad (5.1.1b)$$

$$\lambda_{n,k}(x) = \frac{\omega_n(x)}{(\frac{\partial}{\partial x} \omega_n(x_{n,k})) (x - x_{n,k})} \text{ for } k = 0, 1, \dots, n \quad (5.1.1c)$$

$$A_{n,k} = \int_a^b \lambda_{n,k}(x) dx = \frac{(b-a)(-1)^{(n-k)}}{n k! (n-k)!} \int_0^n \prod_{j=0, j \neq k}^n (t-j) dt \text{ for } k = 0, 1, \dots, n \quad (5.1.1d)$$

With parameters defined in this way, the quadrature in sense of Newton-Cotes is defined as following:

$$NC_n(f) = A_{n,k} \sum_{k=0}^n \left(a + \frac{(b-a)}{n} k \right). \quad (5.1.2)$$

Let's remind the Hilbert transform from the equation (2.1.2):

$$\mathcal{H}[f(x)] = \frac{1}{\pi} \int_{-\infty}^{\infty} \frac{f(\omega)}{(x-\omega)} d\omega. \quad (5.1.3)$$

We would like to apply the Newton-Cotes quadrature to calculate the Hilbert transform. While the NC quadrature is not perfect, we need perform the integration without including a short region $[x-cs, x+cs]$ near the singularity. We will also omit the infinities and instead of them we will integrate from a starting point a to the ending point b .

$$HNC \quad \mathcal{H}_{NC}[f(x)] \approx \frac{1}{\pi} \int_a^{x-cs} \frac{f(\omega)}{(x-\omega)} d\omega + \frac{1}{\pi} \int_{x+cs}^b \frac{f(\omega)}{(x-\omega)} d\omega. \quad (5.1.4)$$

Parameters such as a , b and cs are widely described the Appendix A.2 with the whole source code and additional comments.

cs to jeden symbol, ay ibayn cs?

Pozbudoval

ω to tol ??

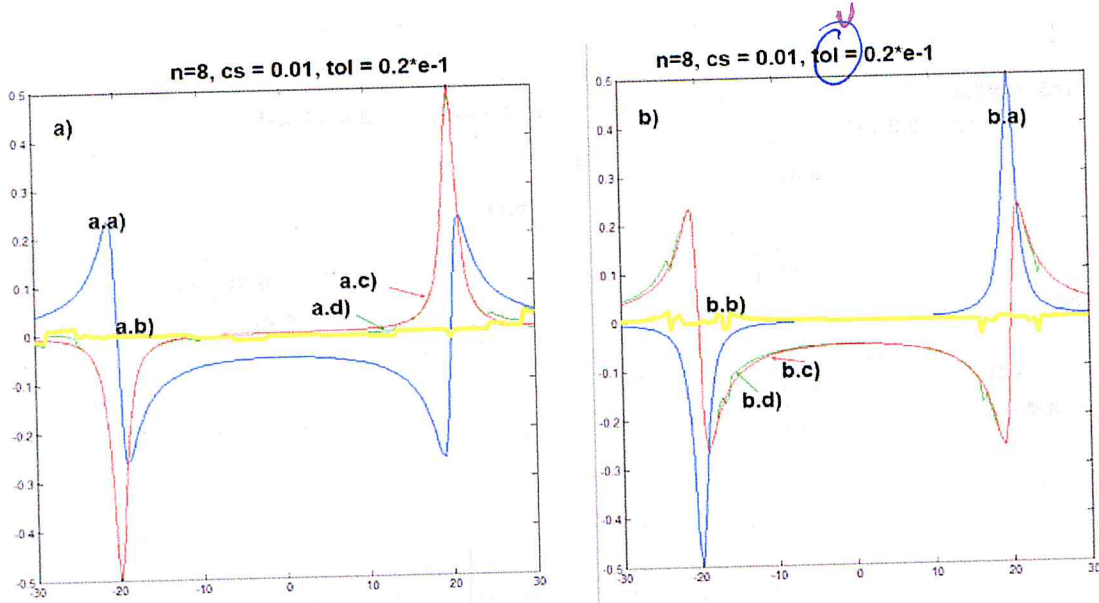


Figure 5.2.1: The Figure presents the first of four results of the NC Hilbert Transform method applied for the simple linear model. Results are plotted together. Calculations were performed with the parameters ($n = 8$, $cs = .1e-1$, $tol = .2e-1$)
 a.a) The plot of the real part of $\chi(\omega)$
 a.b) absolute error plot (a.d-plot minus a.c-plot)
 a.c) imaginary part of $\chi(\omega)$ calculated analytically
 a.d) imaginary part of $\chi(\omega)$ obtained with the NC Hilbert transform of a.a-plot,
 b.a) The plot of the imaginary part of $\chi(\omega)$
 b.b) absolute error with the NC Hilbert transform of a.a-plot, b.a)
 b.c) real part of $\chi(\omega)$ calculated analytically
 b.d) real part of $\chi(\omega)$ obtained with the NC Hilbert transform of b.a-plot

5.2 NC for simple linear model - results

As the prepared numeric method depends on many input parameter arguments, we have tried to perform the evaluation in many different cases, some of those results are stated below. We have used the same model as in chapter 4.2.

$$\chi(\omega) \approx \frac{-20}{(\omega i + 1 - 20 i)(\omega i + 1 + 20 i)} \quad (5.2.1)$$

Some results has been presented on the Figures 5.2.1, 5.2.2, 5.2.3 and 5.2.4

We cannot tell with a hundred percent confidence which set of parameters will fit the best any given function and the user will need to try many combinations before obtaining the final plot, but what we gave is the opportunity to set each one parameter manually, which may lead to better results in the particular cases.

5.3 NC for simple nonlinear model - results

We have performed calculations for the same both nonlinear pump-probe and wave-mixing model as in the chapter 4.2. We have assigned some randomly picked values to the constants:

$$G = 1, \gamma_{ba} = -0.1, n_0 = 1, \Delta = 1.3, \eta = 1, \theta = 1.4, \Omega_1 = 4.3, \Omega_2 = 1, w_0 = 1, h = 1, \mu_{ba} = 1, T_1 = 1, \varepsilon_0 = 1,$$

and we will use them in the pump-and-probe (5.3.1) and the frequency mixing (5.3.2) model equations:

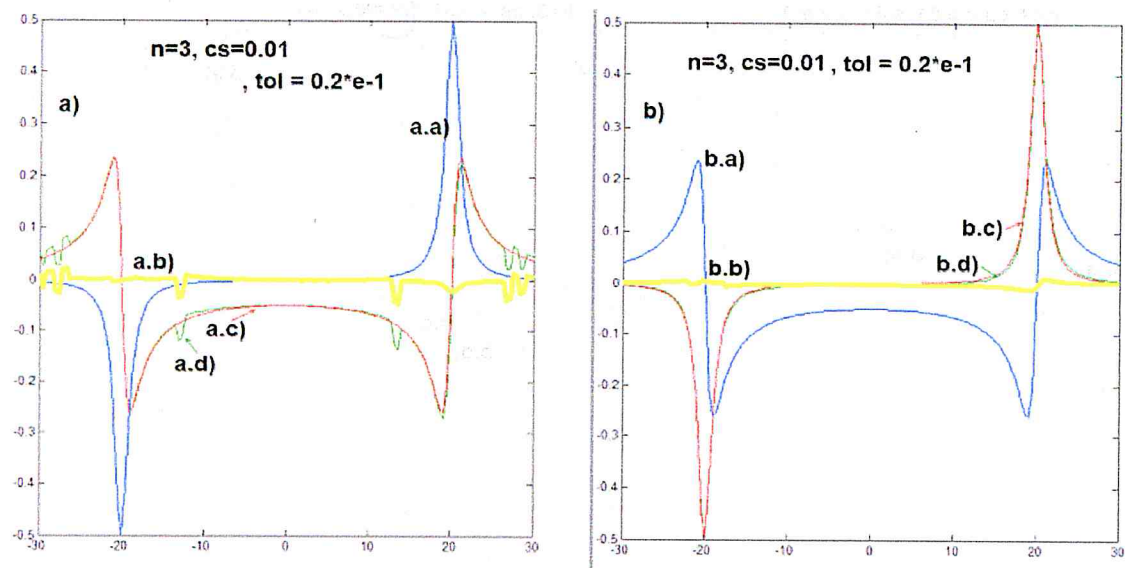


Figure 5.2.2: The Figure presents the second of four results of the NC Hilbert Transform method applied for the simple linear model. Results are plotted together. Calculations were performed with the parameters ($n = 3$, $cs = .1e-1$, $tol = .2e-1$). a.a) The plot of the imaginary part of $\chi(\omega)$ a.b) absolute error plot (a.d-plot minus a.c-plot) a.c) real part of $\chi(\omega)$ calculated analytically a.d) real part of $\chi(\omega)$ obtained with the NC Hilbert transform of a.a-plot, b.a) The plot of the real part of $\chi(\omega)$ b.b) absolute error plot (b.d-plot minus b.c-plot) b.c) imaginary part of $\chi(\omega)$ calculated analytically b.d) imaginary part of $\chi(\omega)$ obtained with the NC Hilbert transform of b.a-plot

↪
↑
usechre
u

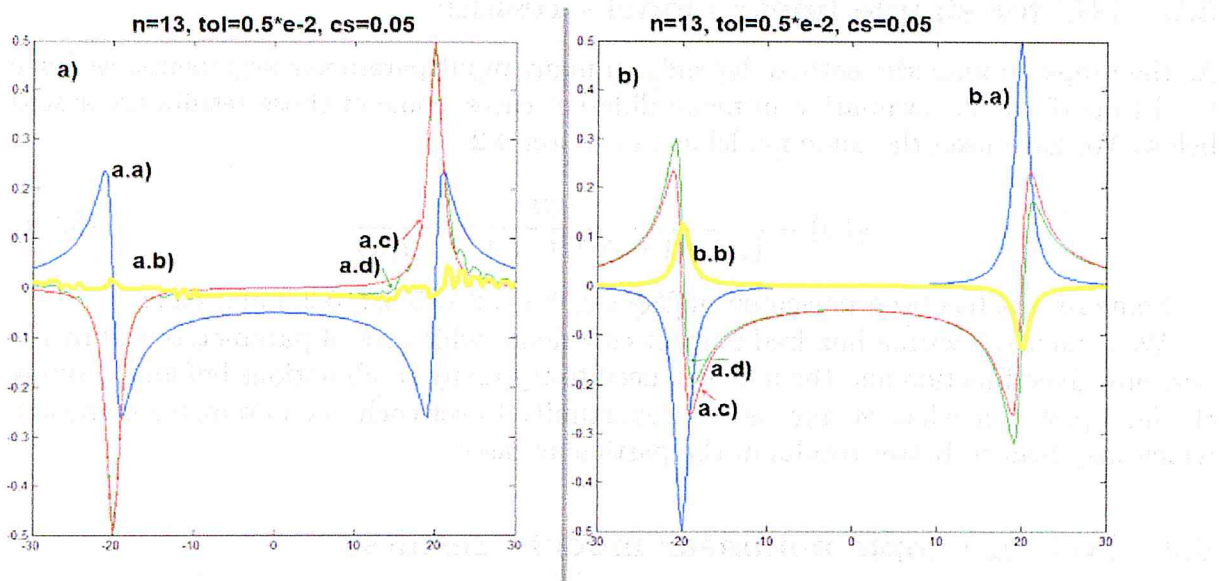


Figure 5.2.3: The Figure presents the third of four results of the NC Hilbert Transform method applied for the simple linear model. Results are plotted together. Calculations were performed with the parameters ($n = 13$, $tol = .5e-2$, $cs = .5e-1$). a.a) The plot of the real part of $\chi(\omega)$ a.b) absolute error plot (a.d-plot minus a.c-plot) a.c) imaginary part of $\chi(\omega)$ calculated analytically a.d) imaginary part of $\chi(\omega)$ obtained with the NC Hilbert transform of a.a-plot, b.a) The plot of the imaginary part of $\chi(\omega)$ b.b) absolute error plot (b.d-plot minus b.c-plot) b.c) real part of $\chi(\omega)$ calculated analytically b.d) real part of $\chi(\omega)$ obtained with the NC Hilbert transform of b.a-plot

↗

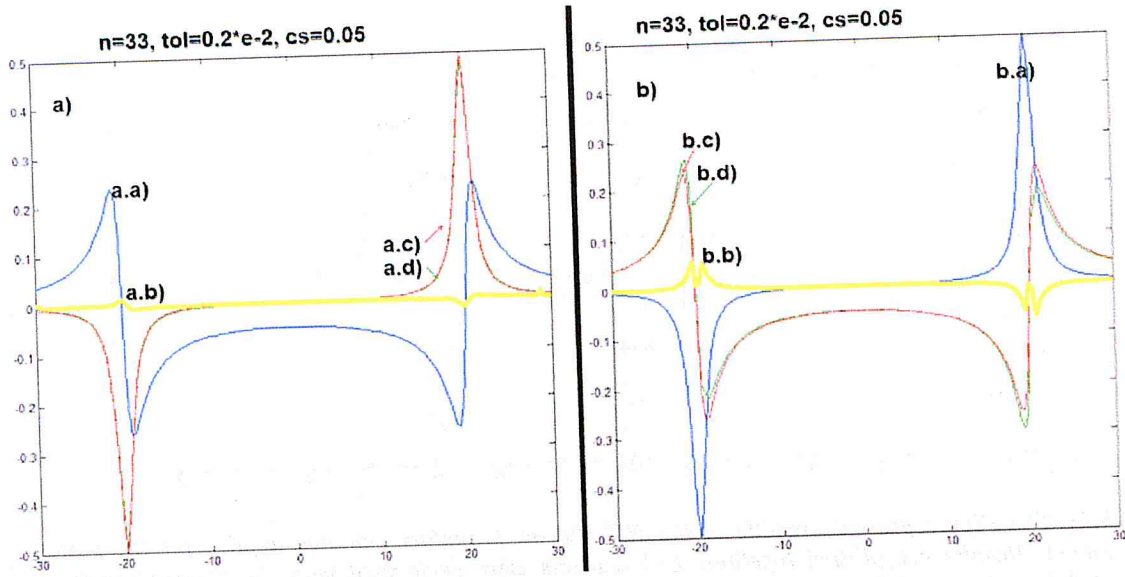


Figure 5.2.4: The Figure presents the fourth of four results of the NC Hilbert Transform method applied for the simple linear model. Results are plotted together. Calculations were performed with the parameters ($n = 33$, $\text{tol} = .2e-2$, $\text{cs} = .5e-1$)
 a.a) The plot of the real part of $\chi(\omega)$
 a.b) absolute error plot ($a.d$ -plot minus $a.c$ -plot)
 a.c) imaginary part of $\chi(\omega)$ calculated analytically
 a.d) imaginary part of $\chi(\omega)$ obtained with the NC Hilbert transform of $a.a$ -plot,
 b.a) The plot of the imaginary part of $\chi(\omega)$
 b.b) absolute error plot ($b.d$ -plot minus $b.c$ -plot)
 b.c) real part of $\chi(\omega)$ calculated analytically
 b.d) real part of $\chi(\omega)$ obtained with the NC Hilbert transform of $b.a$ -plot

$$\chi_{pp}(\delta) = \frac{G n_0 \gamma_{ba}}{\Delta + \delta + I\eta} \left(t_g(\omega) \text{ referring to } d \right) \quad (5.3.1)$$

$$\left(1 - \frac{\Omega_1^2 (\Delta - \delta + I\eta)(\delta + 2I\eta)}{2(\Delta - I\eta)((\delta + I\theta)(\Delta + \delta + I\eta)(\delta - \Delta + I\eta) - \Omega_1^2(\delta + I\eta))} \right),$$

$$\chi_{mix}(\delta) = 6 N w_0 \varepsilon_0 h^3 \mu_{ba}^4 (-\delta - \Delta - \frac{i}{T_2}) (\delta + \frac{2i}{T_2})(\Delta + \frac{i}{T_2})(\Delta + \delta + \frac{i}{T_2}) \cdot \quad (5.3.2)$$

$$\cdot (\delta^3 - \frac{2i\delta^2}{T_2} - \delta\Delta^2 - \frac{2i\delta}{T_1 T_2} - \frac{\delta}{T_2^2} + \frac{\delta^2}{T_1} - \frac{\Delta^2}{T_1} - \frac{1}{T_1 T_2^2} - \Omega_2 \delta + \frac{\Omega_2 i}{T_2}).$$

Results for pump-and-probe model has been presented in ~~the~~ Figure 5.3.1. Results for the frequency mixing model has been presented in ~~the~~ Figure 5.3.2.

5.4 NC for simple quantum-perturbative model - results

Linear model - results:

For the linear susceptibility we have used the model from the (3.5):

$$\chi_{1,qp}(\omega) = \frac{N}{\varepsilon_0 h} \sum_{n=1}^2 \left(\frac{\mu_{1,n} \mu_{2,n}}{\Omega_n - \omega - i\gamma_n} + \frac{\mu_{2,n} \mu_{1,n}}{\Omega_n + \omega + i\gamma_n} \right) \quad (5.4.1)$$

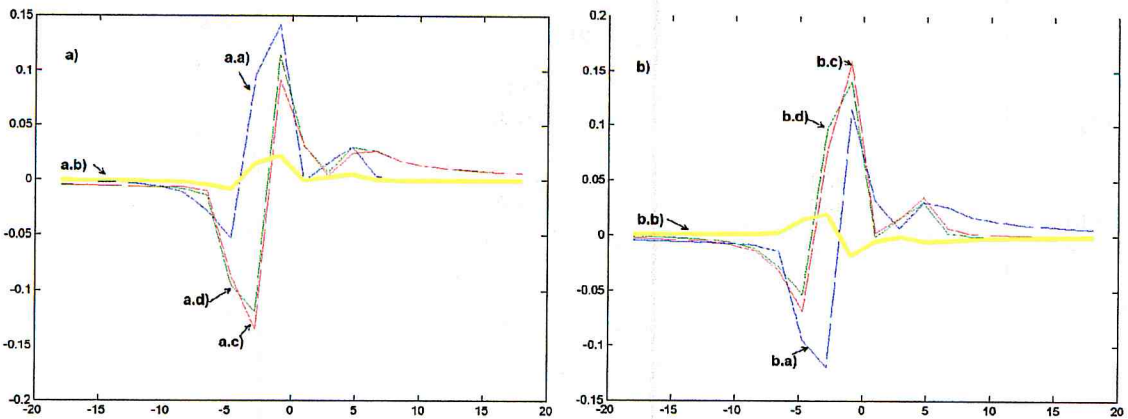


Figure 5.3.1: The Figure presents results of the NC Hilbert Transform method applied for the pump-and-probe model. Results are plotted together. Calculations were performed with the parameters ($n = 4$, $cs = .1e-1$, $tol = .1e-1$) a.a) The plot of the real part of $\chi_{pp}(\omega)$ a.b) absolute error plot (a.d-plot minus a.c-plot) a.c) imaginary part of $\chi_{pp}(\omega)$ calculated analytically a.d) imaginary part of $\chi_{pp}(\omega)$ obtained with the NC Hilbert transform of a.a-plot, b.a) The plot of the imaginary part of $\chi_{pp}(\omega)$ b.b) absolute error plot (b.d-plot minus b.c-plot) b.c) real part of $\chi_{pp}(\omega)$ calculated analytically b.d) real part of $\chi_{pp}(\omega)$ obtained with the NC Hilbert transform of b.a-plot

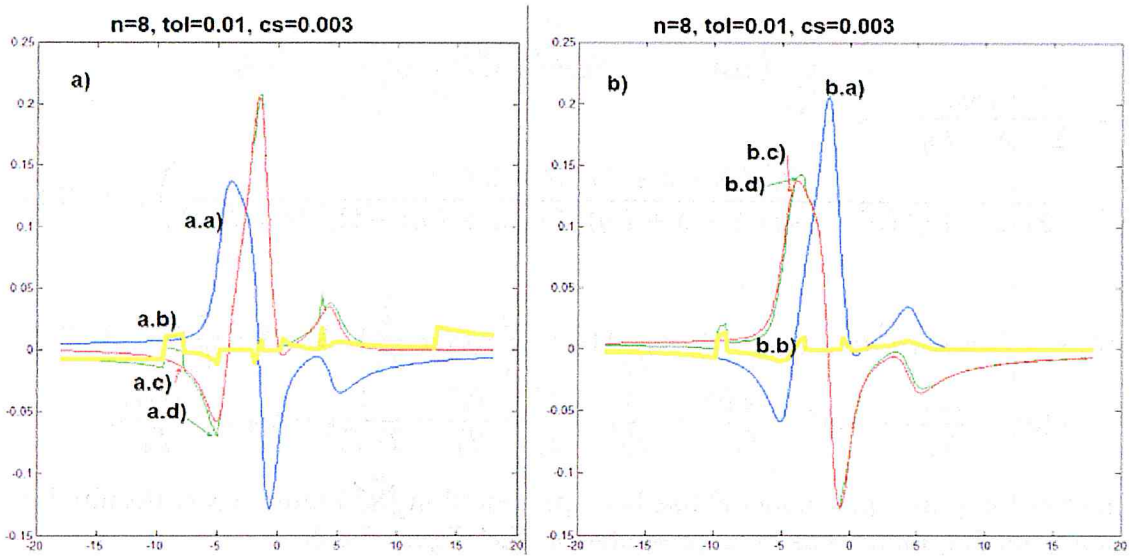


Figure 5.3.2: The Figure presents results of the NC Hilbert Transform method applied for the frequency mixing model. Results are plotted together. Calculations were performed with the parameters ($n = 8$, $cs = .3e-2$, $tol = .1e-1$) a.a) The plot of the real part of $\chi_{mix}(\omega)$ a.b) absolute error plot (a.d-plot minus a.c-plot) a.c) imaginary part of $\chi_{mix}(\omega)$ calculated analytically a.d) imaginary part of $\chi_{mix}(\omega)$ obtained with the Hilbert transform of a.a-plot, b.a) The plot of the imaginary part of $\chi_{mix}(\omega)$ b.b) absolute error plot (b.d-plot minus b.c-plot) b.c) real part of $\chi_{mix}(\omega)$ calculated analytically b.d) real part of $\chi_{mix}(\omega)$ obtained with the Hilbert transform of b.a-plot

Należałoby skończyć z tą częścią, ale fyzycznie to nie może oznaczać, że algorytm NC jest stabilny. Taka implementacja jest dość wstępną i nie ma żadnych gwarancji. Nie wiem jaka będzie jest dla zaakceptowanych z przedziałów punktów widzenia itp...

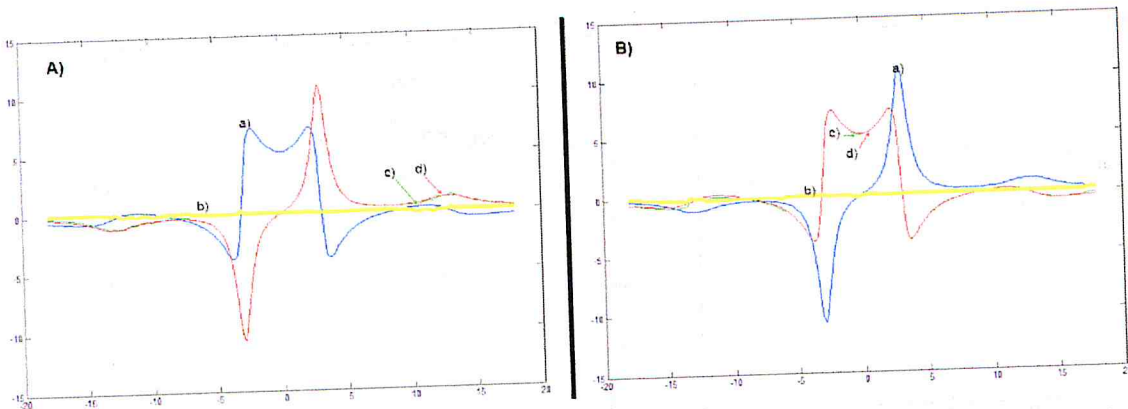


Figure 5.4.1: The Figure presents results of the NC Hilbert Transform method applied for the simple quantum-perturbative model. Results are plotted together. a.a) The plot of the imaginary part of $\chi_{1,qp}(\omega)$ obtained with the NC Hilbert transform of a-plot a.b) absolute error plot (d-plot minus c-plot) a.c) real part of $\chi_{1,qp}(\omega)$ obtained with the NC Hilbert transform of a-plot a.d) real part of $\chi_{1,qp}(\omega)$ calculated analytically b.b) The plot of the real part of $\chi_{1,qp}(\omega)$ b.b) absolute error plot (d-plot minus c-plot) b.c) imaginary part of $\chi_{1,qp}(\omega)$ obtained with the NC Hilbert transform of a-plot b.d) imaginary part of $\chi_{1,qp}(\omega)$ calculated analytically

This time we used the following parameters: $\mu = [[3, -0.5], [1.2, 2.4]]$, $\Omega = [-3, 13]$, $\gamma = [0.7, 2.3]$, $N = 8$, $\varepsilon_0 = 1.4$, $h = -2.7$.

Evaluation time of two plots given in the 5.4.1 was 615 seconds.

Second-order model - results:

For the second-order susceptibility we used the model from the 3.5:

*Eq. (3.5) → chapter
the ω 3.5?*

$$\begin{aligned}
 \chi_{2,qp}(\omega_1, \omega_2) = 2N\varepsilon_0 h^2 \sum_{n=1}^2 \sum_{m=1}^2 \sum_{l=1}^2 & \left(\frac{\mu_{l,n} \mu_{nm} \mu_{ml}}{(\Omega_{nl} - \omega_1 - \omega_2 - i\gamma_{nl})(\Omega_{ml} - \omega_1 - i\gamma_{ml})} + \right. \\
 & + \frac{\mu_{l,n} \mu_{nm} \mu_{ml}}{(\Omega_{nl} - \omega_1 - \omega_1 - i\gamma_{nl})(\Omega_{ml} - \omega_2 - i\gamma_{ml})} + \\
 & + \frac{\mu_{l,n} \mu_{nm} \mu_{ml}}{(\Omega_{mn} - \omega_1 - \omega_2 - i\gamma_{mn})(\Omega_{nl} + \omega_2 + i\gamma_{nl})} + \\
 & + \frac{\mu_{l,n} \mu_{nm} \mu_{ml}}{(\Omega_{mn} - \omega_1 - \omega_2 - i\gamma_{mn})(\Omega_{nl} + \omega_2 + i\gamma_{nl})} + \\
 & + \frac{\mu_{l,n} \mu_{nm} \mu_{ml}}{(\Omega_{nm} + \omega_1 + \omega_2 + i\gamma_{nm})(\Omega_{ml} - \omega_1 - i\gamma_{ml})} + \\
 & + \frac{\mu_{l,n} \mu_{nm} \mu_{ml}}{(\Omega_{nm} + \omega_1 + \omega_2 + i\gamma_{nm})(\Omega_{ml} - \omega_1 - i\gamma_{ml})} + \\
 & + \frac{\mu_{l,n} \mu_{nm} \mu_{ml}}{(\Omega_{ml} + \omega_1 + \omega_2 + i\gamma_{ml})(\Omega_{nl} + \omega_1 + i\gamma_{nl})} + \\
 & \left. + \frac{\mu_{l,n} \mu_{nm} \mu_{ml}}{(\Omega_{ml} + \omega_1 + \omega_2 + i\gamma_{ml})(\Omega_{nl} + \omega_2 + i\gamma_{nl})} \right) \quad (5.4.2)
 \end{aligned}$$

wijgden
gaat od an-
do our
pyramids!

W2SV

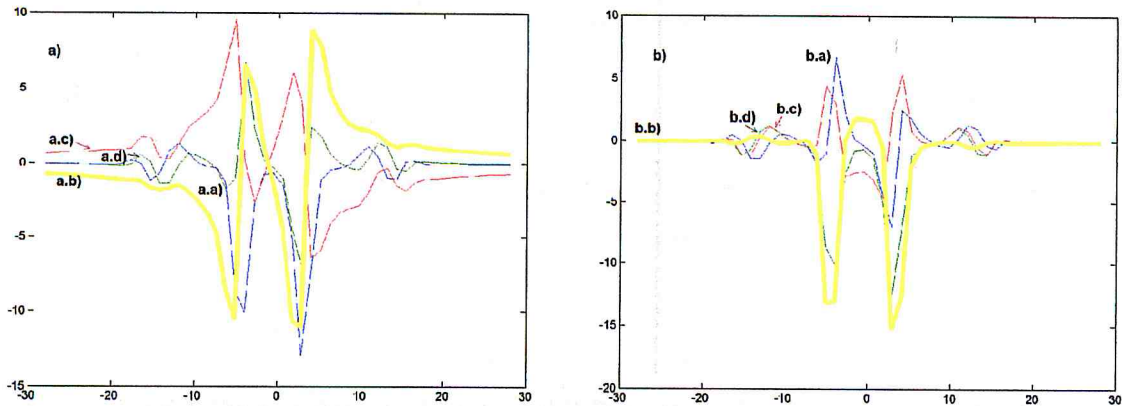


Figure 5.4.2: The Figure presents the results of the NC Hilbert Transform method applied for the second-order quantum-perturbative model. Results are plotted together. Calculations were performed with the parameters ($n = 4$, $cs = .1e-1$, $tol = .1e-1$).
 a.a) The plot of the real part of $\chi_{2,qp}(\omega)$.
 a.b) absolute error plot (a.d-plot minus a.c-plot).
 a.c) imaginary part of $\chi_{2,qp}(\omega)$ calculated analytically.
 a.d) imaginary part of $\chi_{2,qp}(\omega)$ obtained with the NC Hilbert transform of a.a-plot.
 b.a) The plot of the imaginary part of $\chi_{2,qp}(\omega)$.
 b.b) absolute error plot (b.d-plot minus b.c-plot).
 b.c) real part of $\chi_{2,qp}(\omega)$ calculated analytically.
 b.d) real part of $\chi_{2,qp}(\omega)$ obtained with the NC Hilbert transform of b.a-plot.

with the constant values already chosen:

$$\mu = \begin{vmatrix} 1 & 3 \\ -1 & -2 \end{vmatrix}, \quad \Omega = \begin{vmatrix} 3 & 16 \\ 4 & 12 \end{vmatrix}, \quad \gamma = \begin{vmatrix} 1 & 2 \\ -1 & 3 \end{vmatrix}, \quad N = 5, \quad \varepsilon_0 = 1, \quad h = -1.$$

Results are presented in the Figure 5.4.2. We can see a very large relative error reaching up to the 100%. We can also see that this model seems to be invalid. This will be checked with another methods in next chapters.

6 Hilbert Clenshaw-Curtis Implementation

6.1 Overview of the Hilbert Clenshaw-Curtis Implementation

The algorithm for the Hilbert transform using the modified Clenshaw-Curtis quadrature is presented.

Clebsch-Curtis quadrature:

The heart of the calculation has been presented by T. Hasegawa and T. Torri in [15]. First we will need to calculate the Cauchy principal value integral on the interval $[-1, 1]$:

$$\int_{-1}^1 \frac{f(x)}{(x-c)} dx \text{ for } c \in (-1, 1). \quad (6.1.1)$$

The first step suggested by the authors is to remove the singularity from the integral (Eq. 6.1.2):

$$\int_{-1}^1 \frac{f(x)}{(x-c)} dx = \int_{-1}^1 \frac{f(x) - f(c)}{(x-c)} + f(c) \log\left(\frac{1-c}{1+c}\right) \quad (6.1.2)$$

PRZESŁUJĄCY ALGORYTM

After some transformation authors finally obtain the iterative formula presented in the equations 6.1.3a and 6.1.3b. The formula 6.1.3a depends on the parameter N, which will be used in the adaptive algorithm. The recursive equation 6.1.3b should be solved with the starting values: $d_N = d_{N+1} = 0$

$$\int_{-1}^1 \frac{f(x)}{(x-c)} dx \approx 2 \sum_{k=0}^{N/2-1} \frac{d_{2k}}{1-4k^2} + f(c) \log\left(\frac{1-c}{1+c}\right) \quad (6.1.3a)$$

$$d_{k+1} - 2cd + k + d_{k-1} = 2a_k^N \text{ for } k = N, N-1, \dots, 1. \quad (6.1.3b)$$

The remaining issue is to calculate the a_k^N coefficients, which has been described in the equation 6.1.4. It is also known as the discrete cosine transform of the first type (DCT-I):

$$a_k^N = \frac{2}{N} \sum_{j=0}^N f\left(\cos\left(\frac{\pi j}{N}\right)\right) \cos\left(\frac{\pi kj}{N}\right), 0 \leq k \leq N \quad (6.1.4)$$

Hilbert transform using the Clenshaw-Curtis quadrature:

While the Clenshaw-Curtis quadrature is defined for finite range $[-1, 1]$, the Hilbert transform uses the definite and improper integral over the range $[-\infty, \infty]$. Here we must remind the law of conservation of energy, from which we can easily deduce that the susceptibility - as the investigated physical quantity - for low frequencies and thus for low energies has low values. From this it follows that function $f = f(x)$ tends to zero when closing to infinities. Thereby the value of integrated function from equation 6.1.5 decreases rapidly and for relatively large values of x this integrand will be omitted.

$$\frac{f(x)}{x-c} dx \quad \text{co to?} \quad (6.1.5)$$

Therefore, we will not be changing the integration range from interval to real line. What must be taken into consideration right now is that the well-chosen, finite interval for integration stated in 6.1.6 or an integral with a period few times bigger.

$$[A, B] = [a - 2|b-a|, b + 2|b-a|] \quad (6.1.6)$$

The specific choice of integration interval should be done during the numerical calculations. As default in our algorithm, we have set the integration interval to be based on the 6.1.6, but with period simply 5 times longer. For all investigated models it gave us satisfactory results.

Our implementation of the Hilbert Clenshaw-Curtis iterations:

So far we have presented the overview of procedures responsible for evaluation of the Clenshaw-Curtis quadrature and the Hilbert transform using the Clenshaw-Curtis quadrature at one point. But in the typical situation we have the whole vector of function values for a given range of abscissas - so what is left - we perform the single-point Hilbert transform based on the Clenshaw-Curtis quadrature for each given point. But to omit the problems with singularities, we will add some post- and precalculations - using the cubic interpolation. The whole procedure is now:

INPUT:

X, Y - given N -length abscissas and related ordinates
 A, B - extended ranges of the interval (based on Y)

PRE-CALCULATIONS:

$$T = B - A \quad (6.1.7)$$

$$C = \frac{B + A}{2} \quad (6.1.8)$$

From N points of Y we calculate the cubic interpolation having $N - 1$ inner points:

$$Y_{p1} = \frac{3Y_1 + 6Y_2 - Y_3}{8} \quad (6.1.9a)$$

$$Y_{pk} = \frac{-Y_{k-1} + 9Y_k + 9Y_{k+1} - Y_{k+2}}{16} \quad (6.1.9b)$$

$$Y_{pN} = \frac{-Y_{N-2} + 6Y_{N-1} + 3Y_N}{8} \quad (6.1.9c)$$

MAIN CALCULATIONS:

As the central part, we calculate the $N - 1$ values for each one of inner points:

$$d_k = \frac{2(Y_{pk} - C)}{T}, \text{ for } k = 1, \dots, N - 1 \quad (6.1.10)$$

$$Hh_k \approx \frac{1}{\pi} \int_A^B \frac{f(\frac{x-T}{2} + C)}{x - d_k} dx, \text{ for } k = 1, \dots, N - 1 \quad (6.1.11)$$

POST-CALCULATIONS:

From $N - 1$ points of Hh we calculate N points using the reverse cubic interpolation:

$$H_1 = \frac{15Hh_1 - 10Hh_2 + 3Hh_3}{8} \quad (6.1.12a)$$

$$H_2 = \frac{3Hh_1 + 6Hh_2 - Hh_3}{8} \quad (6.1.12b)$$

$$H_k = \frac{-Hh_{k-1} + 9Hh_k + 9Hh_{k+1} - Hh_{k+2}}{16} \quad (6.1.12c)$$

$$H_{N-1} = \frac{-Hh_{N-3} + 6Hh_2 - Hh_3}{8} \quad (6.1.12d)$$

$$H_N = \frac{3Hh_{N-3} - 10Hh_{N-2} + 15Hh_{N-1}}{8} \quad (6.1.12e)$$

OUTPUT:

H - N -length Hilbert transform for given function values at X abscissas

The algorithm source has been presented in the Appendix A.3.

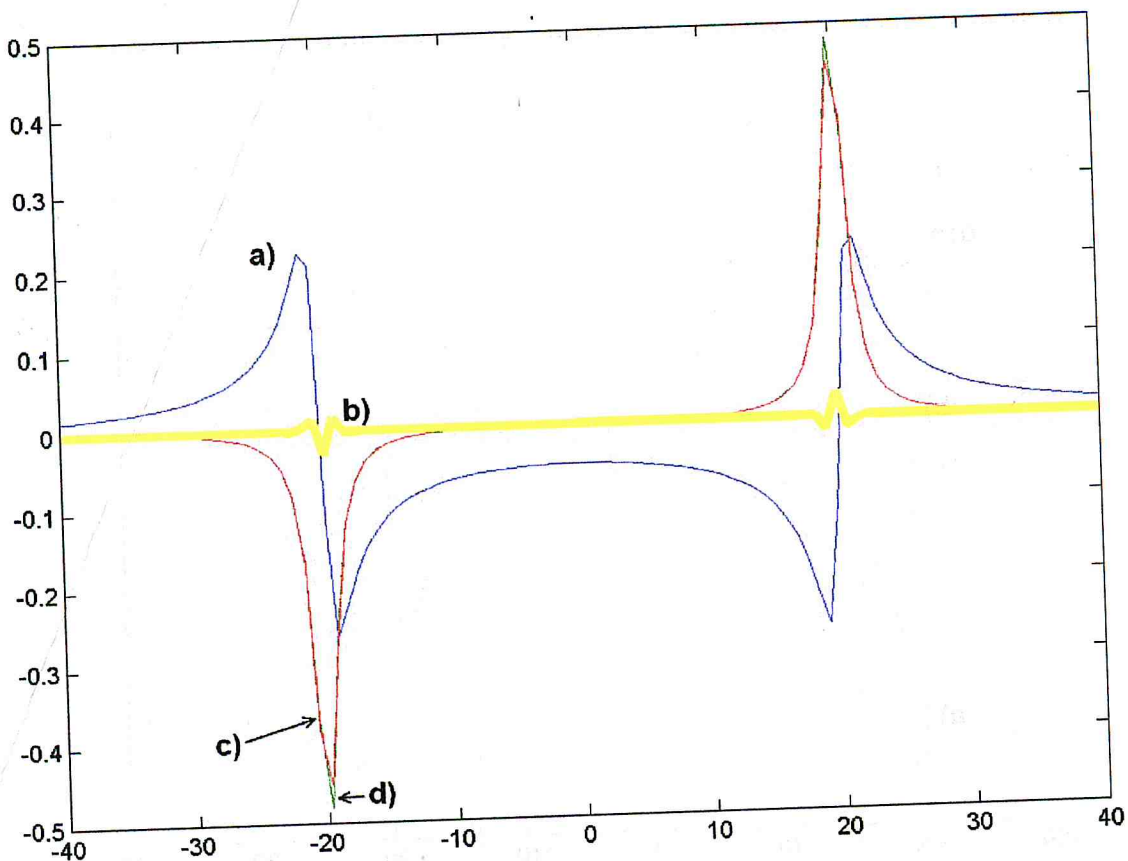


Figure 6.2.1: The Figure presents the results of the Hilbert Clenshaw-Curtis iterations method applied to the real part of the simple linear model. Results are plotted together. a) The plot of the real part of $\chi(\omega)$ b) absolute error plot (c-plot minus d-plot) c) imaginary part of $\chi(\omega)$ obtained with the Hilbert transform of a-plot d) imaginary part of $\chi(\omega)$ calculated analytically.

6.2 HCCI for simple linear model

The Figures 6.2.1 and 6.2.2 presents the results obtained with the method for the model defined in model 3.3.3. As we can see - the Hilbert Clenshaw-Curtis iterations gives us much better accuracy than HTRAN or Newton-Cotes quadrature. In next chapters we will check what happens for another models.

6.3 HCCI for simple nonlinear model

For the pump-probe and frequency mixing models we have used the same parameters as in chapter 5.3. The results obtained with the Hilbert Clenshaw-Curtis iterations has been presented in Figures 6.3.1 and 6.3.2 respectively.

As we can see here - once again the results come with quite well accuracy.

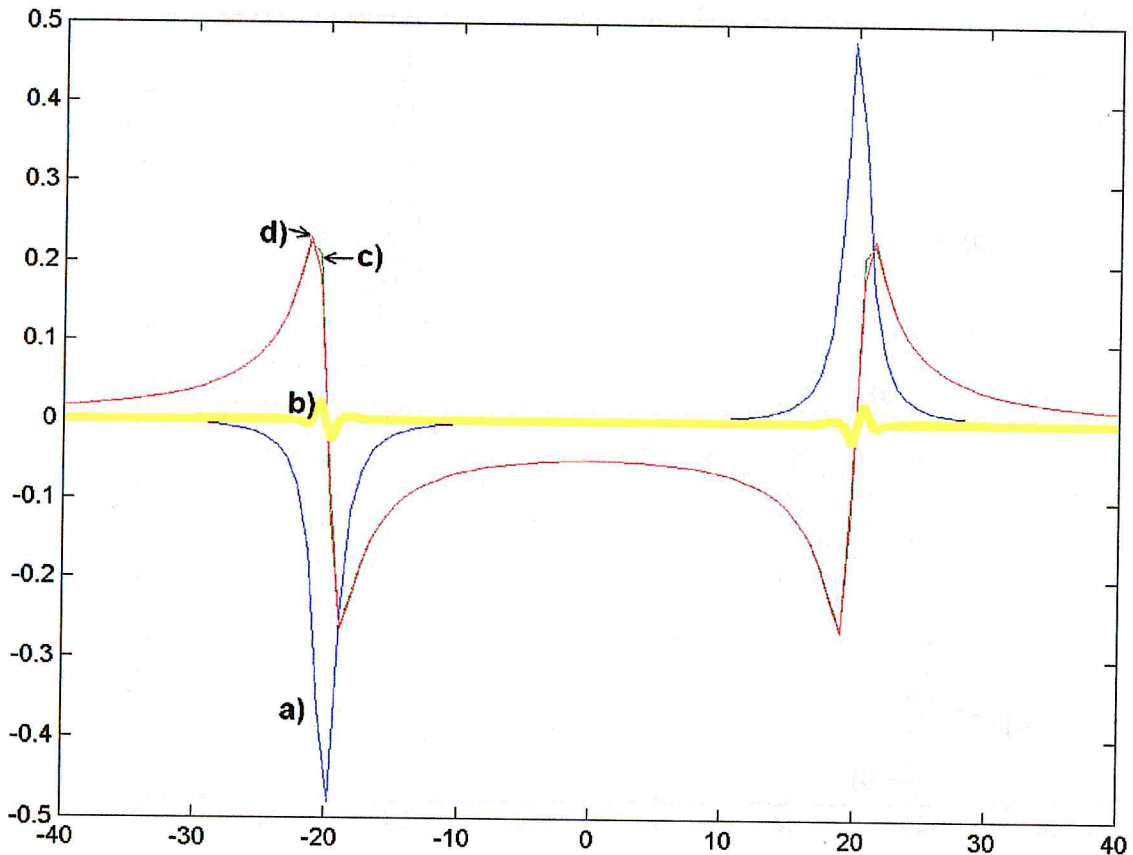


Figure 6.2.2: The Figure presents the results of the Hilbert Clenshaw-Curtis iterations method applied to the imaginary part of the simple linear model. Results are plotted together. a) The plot of the imaginary part of $\chi(\omega)$ b) absolute error plot (c-plot minus d-plot) c) real part of $\chi(\omega)$ obtained with the Hilbert transform of a-plot d) real part of $\chi(\omega)$ calculated analytically.

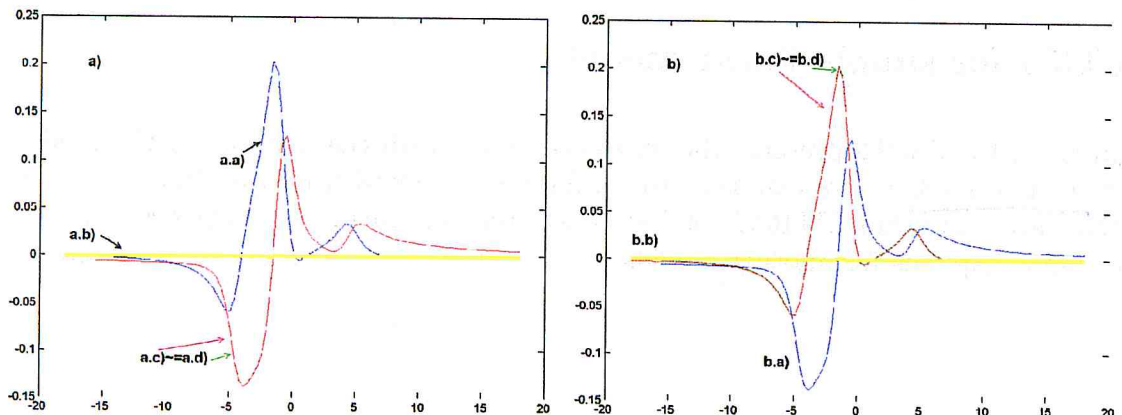


Figure 6.3.1: Results for the pump-probe model using the Hilbert Clenshaw-Curtis iterations a.a) The plot of the real part of $\chi_{pp}(\delta)$ a.b) absolute error plot (a.d-plot minus a.c-plot) a.c) imaginary part of $\chi_{pp}(\delta)$ calculated analytically a.d) imaginary part of $\chi_{pp}(\delta)$ obtained with the Hilbert transform of a.a-plot, b.a) The plot of the imaginary part of $\chi_{pp}(\delta)$ b.b) absolute error plot (b.d-plot minus b.c-plot) b.c) real part of $\chi_{pp}(\omega)$ calculated analytically b.d) real part of $\chi_{pp}(\delta)$ obtained with the Hilbert transform of b.a-plot

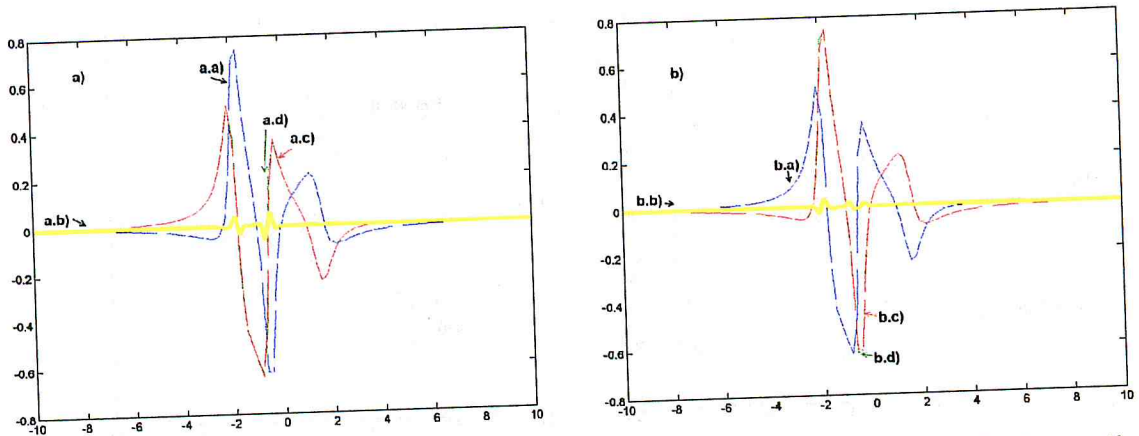


Figure 6.3.2: Results for the frequency mixing model using the Hilbert Clenshaw-Curtis iterations
 a) The plot of the real part of $\chi_{mix}(\delta)$ a.b) absolute error plot (a.d-plot minus a.c-plot) a.c) imaginary part of $\chi_{mix}(\delta)$ calculated analytically a.d) imaginary part of $\chi_{mix}(\delta)$ obtained with the Hilbert transform of $\chi_{mix}(\delta)$
 b) The plot of the imaginary part of $\chi_{mix}(\delta)$ b.b) absolute error plot (b.d-plot minus b.c-plot) b.a) The plot of the imaginary part of $\chi_{mix}(\delta)$ b.b) absolute error plot (b.d-plot minus b.c-plot, b.a) The plot of the imaginary part of $\chi_{mix}(\delta)$ b.b) absolute error plot (b.d-plot minus b.c-plot) b.c) real part of $\chi_{mix}(\omega)$ b.d) real part of $\chi_{mix}(\delta)$ obtained with the Hilbert transform of b.a-plot

6.4 HCCI for simple quantum-perturbative model

Linear model - results:

As in the Chapter 5.3, we have used the same model to describe the simple linear quantum-perturbative model:

$$\chi_{1,qp}(\omega) = \frac{N}{\varepsilon_0 h} \sum_{n=1}^2 \left(\frac{\mu_{1,n} \mu_{2,n}}{\Omega_n - \omega - i\gamma_n} + \frac{\mu_{2,n} \mu_{1,n}}{\Omega_n + \omega + i\gamma_n} \right) \quad (6.4.1)$$

This time we used the following parameters:
 $\mu = [[3, -0.5], [1.2, 2.4]]$, $\Omega = [-3, 13]$, $\gamma = [0.7, 2.3]$, $N = 8$, $\varepsilon_0 = 1.4$, $h = -2.7$.

Results are presented in the Figure 6.4.1. We can see a perfect match here!

Second-order model - results:

We have also used the same model as in 5.3 to describe the second-order susceptibility model:

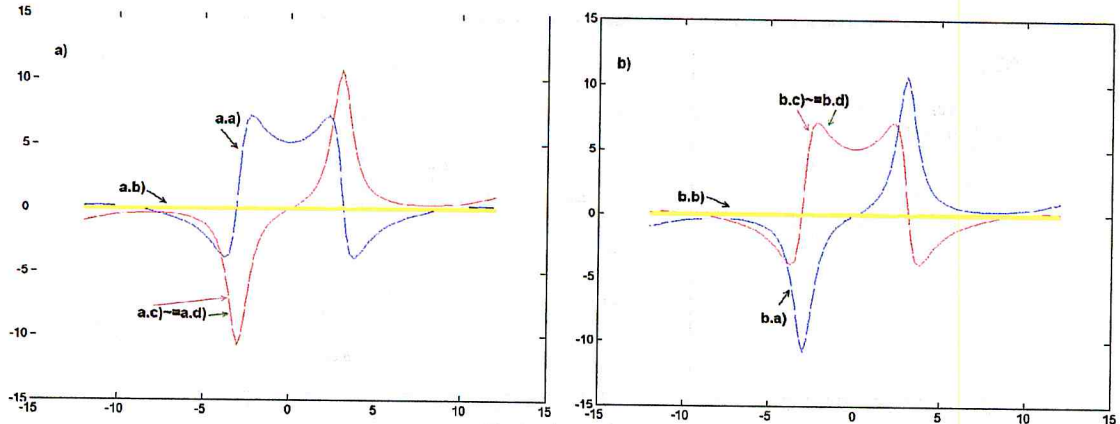


Figure 6.4.1: Results for the linear quantum perturbative model for HCCI quadrature
 a) The plot of the imaginary part of $\chi_{1,qp}(\omega)$
 a.b) absolute error plot (d-plot minus c-plot)
 a.c) real part of $\chi_{1,qp}(\omega)$ obtained with the Hilbert transform of a-plot
 a.d) real part of $\chi_{1,qp}(\omega)$ calculated analytically
 b.b) The plot of the real part of $\chi_{1,qp}(\omega)$
 b.b) absolute error plot (d-plot minus c-plot)
 b.c) imaginary part of $\chi_{1,qp}(\omega)$ obtained with the Hilbert transform of a-plot
 b.d) imaginary part of $\chi_{1,qp}(\omega)$ calculated analytically

$$\begin{aligned}
 \chi_{2,qp}(\omega_1, \omega_2) = & 2N \varepsilon_0 h^2 \sum_{n=1}^2 \sum_{m=1}^2 \sum_{l=1}^2 \left(\frac{\mu_{l,n} \mu_{nm} \mu_{ml}}{(\Omega_{nl} - \omega_1 - \omega_2 - i\gamma_{nl})(\Omega_{ml} - \omega_1 - i\gamma_{ml})} + \right. \\
 & + \frac{\mu_{l,n} \mu_{nm} \mu_{ml}}{(\Omega_{nl} - \omega_1 - \omega_2 - i\gamma_{nl})(\Omega_{ml} - \omega_2 - i\gamma_{ml})} + \\
 & + \frac{\mu_{l,n} \mu_{nm} \mu_{ml}}{(\Omega_{mn} - \omega_1 - \omega_2 - i\gamma_{mn})(\Omega_{nl} + \omega_2 + i\gamma_{nl})} + \\
 & + \frac{\mu_{l,n} \mu_{nm} \mu_{ml}}{(\Omega_{mn} - \omega_1 - \omega_2 - i\gamma_{mn})(\Omega_{nl} + \omega_2 + i\gamma_{nl})} + \\
 & + \frac{\mu_{l,n} \mu_{nm} \mu_{ml}}{(\Omega_{nm} + \omega_1 + \omega_2 + i\gamma_{nm})(\Omega_{ml} - \omega_1 - i\gamma_{ml})} + \\
 & + \frac{\mu_{l,n} \mu_{nm} \mu_{ml}}{(\Omega_{nm} + \omega_1 + \omega_2 + i\gamma_{nm})(\Omega_{ml} - \omega_1 - i\gamma_{ml})} + \\
 & + \frac{\mu_{l,n} \mu_{nm} \mu_{ml}}{(\Omega_{ml} + \omega_1 + \omega_2 + i\gamma_{ml})(\Omega_{nl} + \omega_1 + i\gamma_{nl})} + \\
 & \left. + \frac{\mu_{l,n} \mu_{nm} \mu_{ml}}{(\Omega_{ml} + \omega_1 + \omega_2 + i\gamma_{ml})(\Omega_{nl} + \omega_2 + i\gamma_{nl})} \right) \quad (6.4.2)
 \end{aligned}$$

for the defined set of parameters:

$$\mu = \begin{vmatrix} 1 & 3 \\ -1 & -2 \end{vmatrix}, \quad \Omega = \begin{vmatrix} 3 & 16 \\ 4 & 12 \end{vmatrix}, \quad \gamma = \begin{vmatrix} 1 & 2 \\ -1 & 3 \end{vmatrix}, \quad N = 5, \quad \varepsilon_0 = 1, \quad h = -1$$

Results are presented in the Figure 6.4.2. As for the Newton-Cotes calculations in Chapter 5.4 we can see the model could be invalid because the arisen errors reach up to 100%.

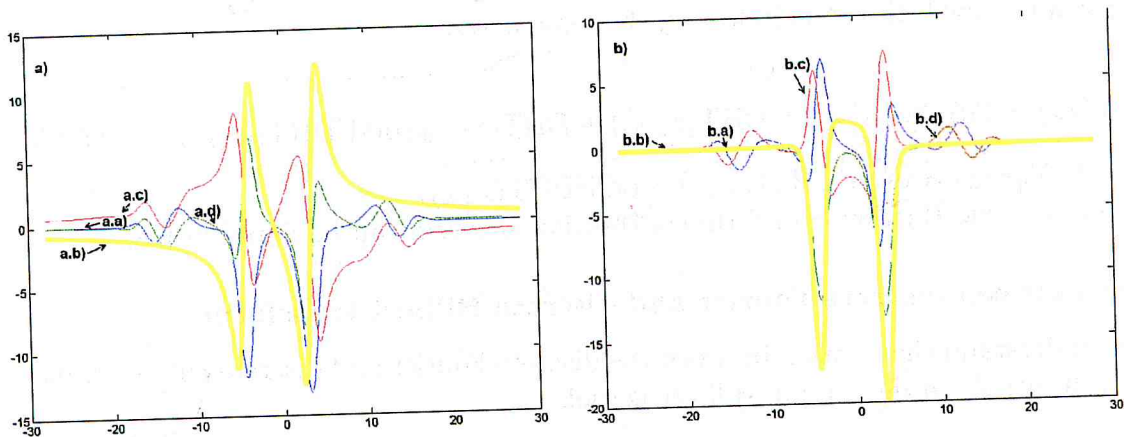


Figure 6.4.2: Results for the second-order quantum perturbative model for HCCI quadrature a.a) The plot of the real part of $\chi_{2,qp}(\omega)$ a.b) absolute error plot (a.d-plot minus a.c-plot) a.c) imaginary part of $\chi_{2,qp}(\omega)$ calculated analytically a.d) imaginary part of $\chi_{2,qp}(\omega)$ obtained with the Hilbert transform of a.a-plot, b.a) The plot of the imaginary part of $\chi_{2,qp}(\omega)$ b.b) absolute error plot (b.d-plot minus b.c-of a.a-plot, b.c) real part of $\chi_{2,qp}(\omega)$ calculated analytically b.d) real part of $\chi_{2,qp}(\omega)$ obtained with the Hilbert transform of b.a-plot

7 Fast Hartley transform approach DHT FHT

7.1 Overview of the FTHA

The Fast Hartley Transform approach for the Hilbert transform is based on two efficient $O(n \log n)$ discrete Hartley transforms and was well described by Soo-Chang Pei in [38]. This approach is faster than another discrete Hilbert transform based on two Fourier transforms, because the whole computation are carried using only real numbers, which is faster than Fourier computation carried using time consuming complex numbers.

Discrete Hartley Transform $X = (X_0, X_1, \dots, X_{N-1})$

For a given N-length vector X both the discrete Hartley transform and inverse discrete Hartley transform are defined as follows:

$$\text{DHT}(X_k) = \sum_{n=0}^{N-1} X_n \left(\cos\left(\frac{2\pi k n}{N}\right) + \sin\left(\frac{2\pi k n}{N}\right) \right) \quad (7.1.1a)$$

$$\text{IDHT}(H_k) = \frac{1}{N} \sum_{k=0}^{N-1} H_k \left(\cos\left(\frac{2\pi k n}{N}\right) + \sin\left(\frac{2\pi k n}{N}\right) \right) \quad (7.1.1b)$$

co to H?

Hartley transform convolution theorem

Now we will introduce the Hartley transform convolution theorem. We define the N-length vector x as convolution of two N-length vectors x_1, x_2 as follows:

$$z_n = x_{1,n} * x_{2,n} = \sum_{k=0}^{N-1} x_{1,k} x_{2,n-k} \quad (7.1.2)$$

zapis najasny

$z = x * v$, gry.

$$z = \sum \dots$$

ω to n ?

ω to n ?

~~$\checkmark \text{ Ev}(X) = [x_0, x_1, x_2, x_3, \dots]$~~ to
 ~~$\checkmark \text{ Od}(\text{--})$~~ For a given convolution, the following theorem is stated:
 even - $[x(4) + x(-4)]/2$
 odd - $[x(4) - x(-4)]/2$
 even ne wyrznic?

$$\text{DHT}(x_n) = \text{DHT}(x_{1,k}) \text{even}(\text{DHT}(x_{2,k})) + \text{DHT}(x_{1,-k}) \text{odd}(\text{DHT}(h_{2,k})), \quad (7.1.3)$$

with: $\text{DHT}(x_{2,k}) = \text{even}(\text{DHT}(x_{2,k})) + \text{odd}(\text{DHT}(x_{2,k}))$

The proof of the Hartley transform convolution theorem can be found in [38].

Relation between discrete Fourier and discrete Hilbert transform

To better understand the relation between the discrete Fourier and discrete Hilbert transform we will introduce the discrete Hilbert kernel:

$$h_k = \frac{1}{\pi k} \text{discrete Hilbert kernel}. \quad (7.1.4)$$

The discrete Fourier transform of the discrete Hilbert kernel will be marked with the symbol $H(k)$:

$$H = \text{DFT}(h)_N$$

$$H(k) = \text{DFT}(h_k), \quad h_k \quad (7.1.5)$$

and the H has the following properties:

$$H(k) = i \text{ for } k = 1, 2, \dots, \frac{N}{2} - 1, \quad (7.1.6a)$$

$$H(k) = 0 \text{ for } k = 0, \frac{N}{2}, \quad (7.1.6b)$$

$$H(k) = -i \text{ for } k = \frac{N}{2} + 1, \frac{N}{2} + 2, \dots, N - 1 \quad (7.1.6c)$$

We derive the discrete Fourier transform of the Hilbert transform for a given N -length vector $x: \in \mathbb{R}^N$

$$Y = \text{DFT}(\text{DHT}(x)) \rightarrow \text{co to?}$$

$$Y_k = H_k \cdot x_k, \quad 2 = \text{DFT}(x)$$

$$\text{DFT}(\text{DISCRETE_HILBERT}(x_k)) = H(k) \text{DFT}(x_k) = (-i) \text{sgn}(k) \text{DFT}(x_k). \quad (7.1.7)$$

Application of the discrete Hartley transform to calculate the discrete Hilbert transform:

Using the Hartley transform convolution theorem (7.1.6) for a given N -length vector x we obtain:

$$\begin{aligned} \text{DHT}(\text{DISCRETE_HILBERT}(x_k)) &= \\ &= \text{DHT}(x_k) \text{even}(\text{DHT}(h_k)) + \text{DHT}(x_{-k}) \text{odd}(\text{DHT}(h_k)), \end{aligned} \quad (7.1.8)$$

where we have used the time reversal notation: $x_{-k} = x_{(N-k) \bmod N}$.

Now we should notice, that the discrete Hilbert transform kernel defined in (7.1.4) is an odd function, so its even part equals zero. So (7.1.8) simplifies now into a product of two separate Hartley transforms:

47 OK

$$\text{DHT}(x_k) \text{DHT}(x)|_k$$

$$\begin{array}{c} \hat{x} \\ \times \\ \text{DHT}(x) \\ \text{DMT}(x) \end{array}$$

$$\text{DHT}(\text{DISCRETE_HILBERT}(x_k)) = \text{DHT}(x_{-k}) \text{odd}(\text{DHT}(h_k)) = \text{DHT}(x_{-k}) \text{DHT}(h_k) \quad (7.1.9)$$

By [38] the second transform is defined: *(to uprowy w p.)*

$$\text{DHT}(h_k) = 1 \text{ for } k = 1, 2, \dots, \frac{N}{2} - 1 \quad (7.1.10a)$$

$$\text{DHT}(h_k) = 0 \text{ for } k = 0, \frac{N}{2} \quad (7.1.10b)$$

$$\text{DHT}(h_k) = -1 \text{ for } k = \frac{N}{2} + 1, \frac{N}{2} + 2, \dots, N - 1 \quad (7.1.10c)$$

In order to calculate the Hilbert of a given N -length vector x the last thing to do is to apply the inverse discrete Hartley transform on the very right side of 7.1.9 equation.

Fast Hartley Transform algorithm

Ronald F. Ullmann has showed the fast algorithm for the discrete Hartley transform in [44]. The important assumption is that ~~as~~ for the fast Fourier transform algorithm, the fast Hartley transform algorithm is defined for a K -length vector x , where K is the power-of-two:

$$\exists p \in \mathbb{N} : K = 2^p \quad \beta = \frac{\pi}{2^{p+1}}, \dots \quad (7.1.11)$$

The 7.1.11 condition for the algorithm and the further possibilities to modify it are discussed further. We will start with the very same thing as in the fast Fourier algorithm - we split the x vector into two smaller vectors:

$$x_{1, \frac{m}{2}} = x_m \text{ for } m = 0, 2, \dots, N - 1 \quad (7.1.12a)$$

$$x_{2, \frac{m-1}{2}} = x_m \text{ for } m = 1, 3, \dots, N - 2 \quad (7.1.12b)$$

Taking into account the initial definition of the discrete Hartley transform 7.1.1a, we obtain:

$$\begin{aligned} \text{DHT}(x_k) &= \left(\sum_{n=0}^{\frac{N}{2}-1} x(2n) \left(\cos\left(\frac{2\pi k 2n}{N}\right) + \sin\left(\frac{2\pi k 2n}{N}\right) \right) \right) + \\ &\quad \left(\sum_{n=0}^{\frac{N}{2}-1} x(2n+1) \left(\cos\left(\frac{2\pi k (2n+1)}{N}\right) + \sin\left(\frac{2\pi k (2n+1)}{N}\right) \right) \right) \end{aligned} \quad (7.1.13)$$

In [44] the following "shift rule" for the discrete Hartley transform is stated :

$$\text{DHT}(x_{k+c}) = \text{DHT}(x_k) \cos(c) + \text{DHT}(x_{-k}) \sin(c) \quad (7.1.14)$$

If we apply the Hartley shift rule 7.1.14 to the split equation in 7.1.13 we obtain:

$$\text{DHT}(x_k) = \text{DHT}(x_{1,k}) + \cos\left(\frac{2\pi k}{N}\right) \text{DHT}(x_{2,k}) + \sin\left(\frac{2\pi k}{N}\right) \text{DHT}(x_{2,-k})$$

for $k = 0, 1, 3, \dots, \frac{N}{2} - 1$ (7.1.15)

The rule 7.1.15 can be applied only for the half of the possible k values ($k < \frac{N}{2}$). Now we will use the periodic properties of the discrete Hartley transform kernel:

$$\cos\left(\frac{2\pi k(n+N)}{N}\right) + \sin\left(\frac{2\pi k 2(n+N)}{N}\right) = \cos\left(\frac{2\pi k n}{N}\right) + \sin\left(\frac{2\pi k 2n}{N}\right) \quad (7.1.16a)$$

$$\cos\left(\frac{2\pi k(n+\frac{N}{2})}{N}\right) + \sin\left(\frac{2\pi k 2(n+\frac{N}{2})}{N}\right) = -\left(\cos\left(\frac{2\pi k n}{N}\right) + \sin\left(\frac{2\pi k 2n}{N}\right)\right) \quad (7.1.16b)$$

The rule 7.1.15 using the periodicity property from 7.1.16 can be now used for all k indices:

$$\text{DHT}(x_k) = \text{DHT}(x_{1,k}) + \cos\left(\frac{2\pi k}{N}\right) \text{DHT}(x_{2,k}) + \sin\left(\frac{2\pi k}{N}\right) \text{DHT}(x_{2,-k}) \quad (7.1.17a)$$

for $k = 0, 1, \dots, \frac{N}{2} - 1$

$$\begin{aligned} \text{DHT}(x_k) = & \\ \text{DHT}(x_{1,k-\frac{N}{2}}) - \cos\left(\frac{2\pi(k-\frac{N}{2})}{N}\right) \text{DHT}(x_{2,k-\frac{N}{2}}) - \sin\left(\frac{2\pi(k-\frac{N}{2})}{N}\right) \text{DHT}(x_{2,-k+\frac{N}{2}}) & \end{aligned} \quad (7.1.17b)$$

for $k = \frac{N}{2}, \frac{N}{2} + 2, \dots, N - 1$

The remaining definition for the negative index, need to be explained:

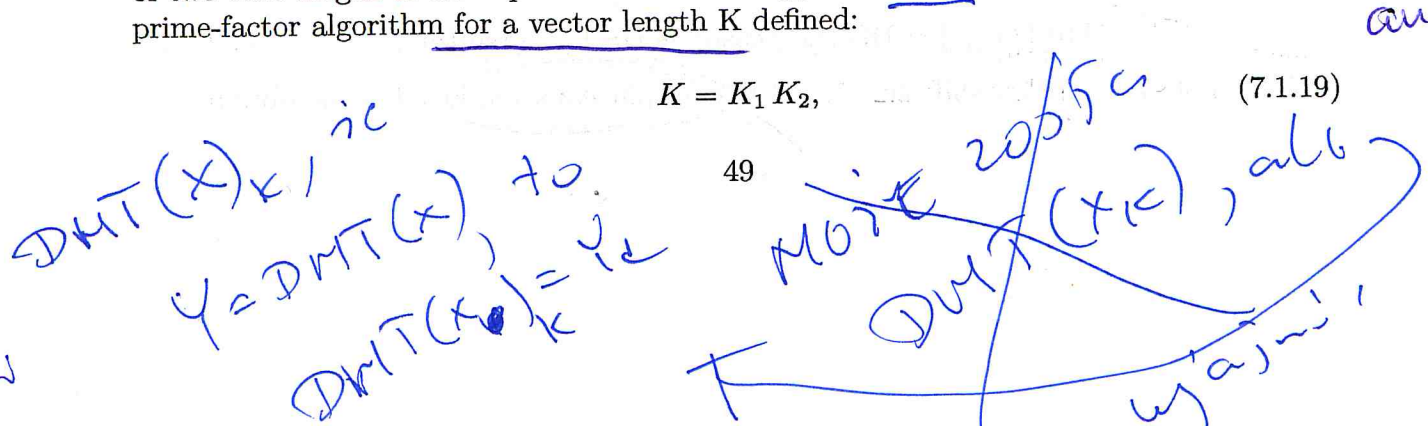
$$\text{DHT}(v_{-k}) = \text{DHT}(v_{(N-k) \bmod N}) \quad (7.1.18)$$

Of course this is a typical divide-and-conquer approach, where the complexity is reduced from $O(n^2)$ to $O(n \log(n))$, very similar to the approach used in the Cooley-Tukey FFT algorithm [11].

Non-power-of-two case

There are several approaches when calculating the fast Fourier transform for a non-power-of-two case length of the input x vector. One approach PFA is the Good-Thomas [13] / prime-factor algorithm for a vector length K defined:

$$K = K_1 K_2, \quad (7.1.19)$$



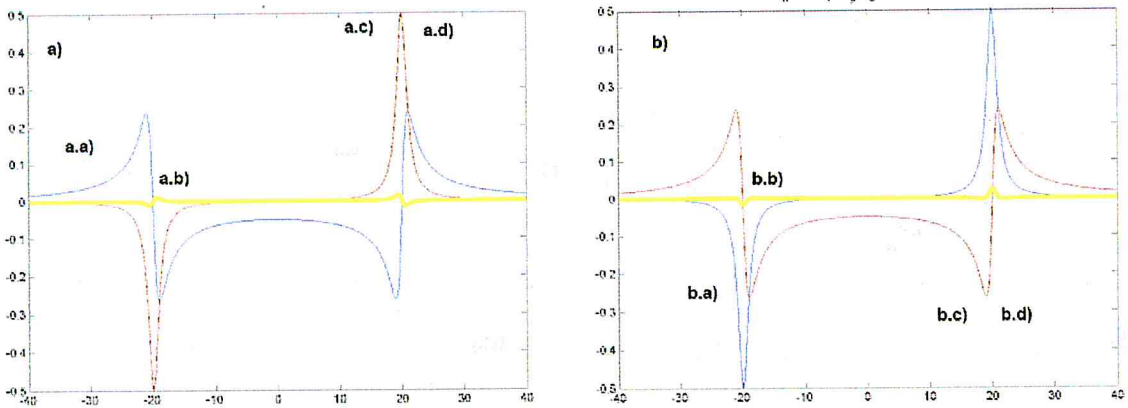


Figure 7.2.1: The Figure presents the results of the Fast Hartley Hilbert Transform method applied to the simple linear model. Results are plotted together. a.a) The plot of the real part of $\chi(\omega)$ a.b) absolute error plot (c-plot minus d-plot) a.c) imaginary part of $\chi(\omega)$ obtained with the Hilbert transform of a-plot a.d) imaginary part of $\chi(\omega)$ calculated analytically. b.a) The plot of the imaginary part of $\chi(\omega)$ b.b) absolute error plot (c-plot minus d-plot) b.c) real part of $\chi(\omega)$ b.d) real part of $\chi(\omega)$ calculated analytically.

Where K_1 and K_2 are relatively prime numbers. Another approach was presented by Leo Bluestein, called also the chirp z-transform algorithm is presented in [2]. Another author, George Bruun, has invented the approach based on the recursive polynomial-factorization in [6]. Rader has prepared the special FFT algorithm especially for vectors of prime size in [33]. But we will use the simplest possible approach - called the zero-padding. So in case of input vector with the size of non-power-of-two, we add the suffix vector filled with vectors to fit the next possible power-of-two size. In the worst case, the input vector size will be doubled, which has no influence on the asymptotic complexity, which remains $O(n \log n)$. While the discrete signal analysis is the domain of scientists, we will end with conclusion stated by M. Lamb in [22] that he is uncertain, if zero padding has an influence on the spectral resolution, but in most cases it has a little influence on the results obtained in the discrete transforms.

The source code of the discrete Hilbert transform using both the fast Hartley transform and inverse fast Hartley transform has been presented in Appendix A.4.

7.2 FTHA for simple linear model

In the Figure 7.2.1 we have presented the results obtained with the Fast Hartley Hilbert Transform for the simple linear model defined in model 3.3.3. As we can see - the Fast Hartley Hilbert Transform gives us quite well accuracy, similar to HCCI and much better than HTRAN or Newton-Cotes quadrature.

7.3 FTHA for simple nonlinear model

For the pump-probe and frequency mixing models we have used the same parameters as in chapter 5.3. The results obtained with the Fast Hartley Hilbert Transform has been presented in Figures 7.3.1 and 7.3.2 respectively.

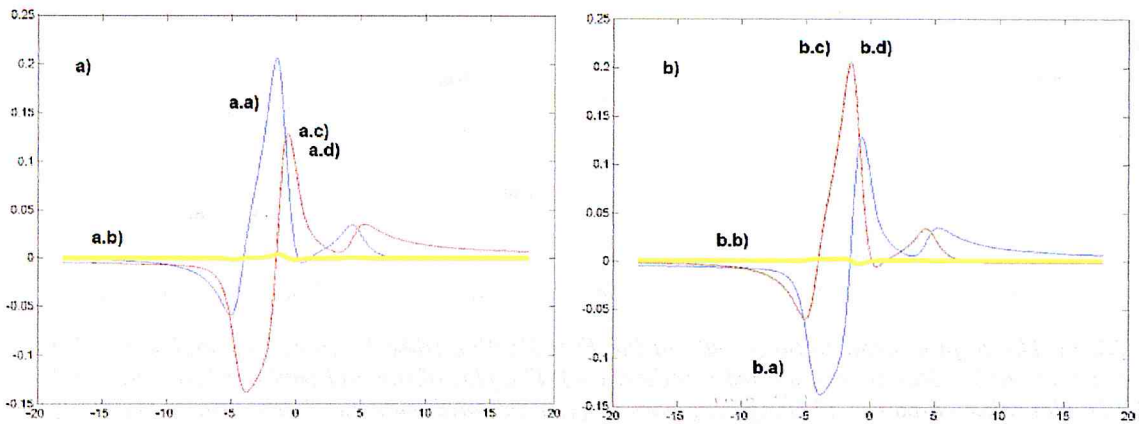


Figure 7.3.1: The Figure presents the results of the Fast Hartley Hilbert Transform method applied to the pump-and-probe model. Results are plotted together. a.a) The plot of the real part of $\chi_{pp}(\omega)$ a.b) absolute error plot (a.d-plot minus a.c-plot) a.c) imaginary part of $\chi_{pp}(\omega)$ calculated analytically a.d) imaginary part of $\chi_{pp}(\omega)$ obtained with the Hilbert transform of a.a-plot, b.a) The plot of the imaginary part of $\chi_{pp}(\omega)$ b.b) absolute error plot (b.d-plot minus b.c-plot) b.c) real part of $\chi_{pp}(\omega)$ calculated analytically b.d) real part of $\chi_{pp}(\omega)$ obtained with the Hilbert transform of b.a-plot

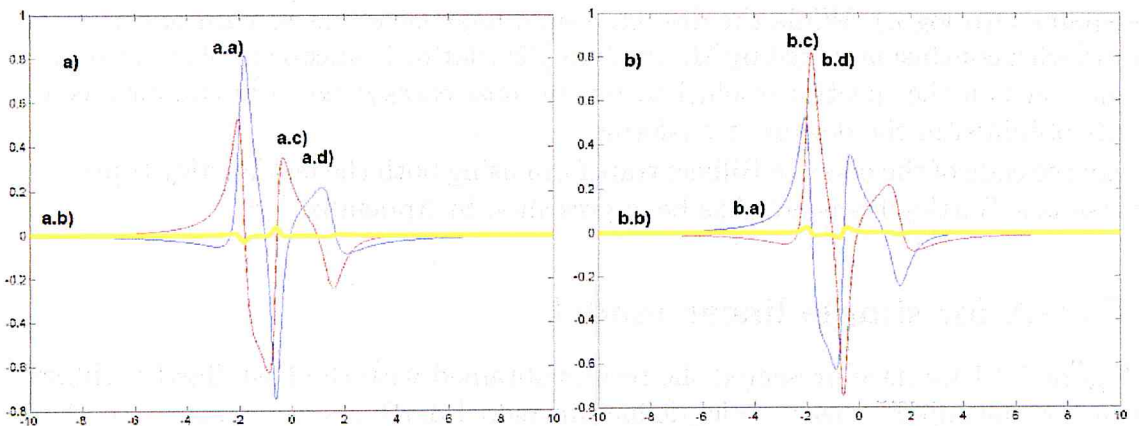


Figure 7.3.2: The Figure presents the results of the Fast Hartley Hilbert Transform method applied to the frequency mixing model. Results are plotted together. a.a) The plot of the real part of $\chi_{mix}(\delta)$ a.b) absolute error plot (a.d-plot minus a.c-plot) a.c) imaginary part of $\chi_{mix}(\omega)$ calculated analytically a.d) imaginary part of $\chi_{mix}(\omega)$ obtained with the Hilbert transform of a.a-plot, b.a) The plot of the imaginary part of $\chi_{mix}(\omega)$ b.b) absolute error plot (b.d-plot minus b.c-plot) b.c) real part of $\chi_{mix}(\omega)$ calculated analytically b.d) real part of $\chi_{mix}(\omega)$ obtained with the Hilbert transform of b.a-plot

a sketch +
done later
W.

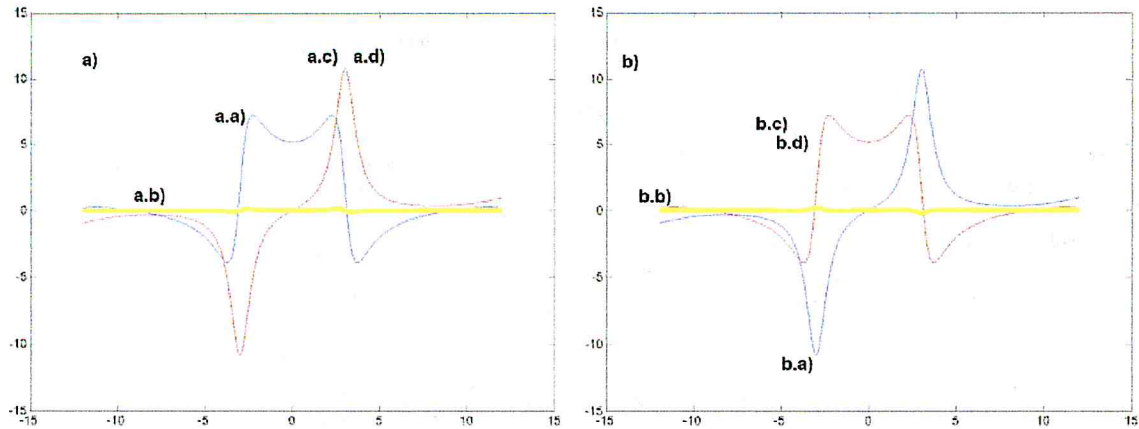


Figure 7.4.1: Results for the linear quantum perturbative model for FHT Hilbert transform *a.a)* The plot of the imaginary part of $\chi_{1,qp}(\omega)$ *a.b)* absolute error plot (*d*-plot minus *c*-plot) *a.c)* real part of $\chi_{1,qp}(\omega)$ obtained with the Hilbert transform of *a*-plot *a.d)* real part of $\chi_{1,qp}(\omega)$ calculated analytically *b.b)* The plot of the real part of $\chi_{1,qp}(\omega)$ *b.b)* absolute error plot (*d*-plot minus *c*-plot) *b.c)* imaginary part of $\chi_{1,qp}(\omega)$ obtained with the Hilbert transform of *a*-plot *b.d)* imaginary part of $\chi_{1,qp}(\omega)$ calculated analytically

Once again we can see a very good accuracy, better than for HTRAN or Newton-Cotes, and similar to HCCI.

7.4 FTHA for simple quantum-perturbative model

Linear model - results:

As in the Chapter 5.3, we have used the same model to describe the simple linear quantum-perturbative model:

$$\chi_{1,qp}(\omega) = \frac{N}{\varepsilon_0 h} \sum_{n=1}^2 \left(\frac{\mu_{1,n} \mu_{2,n}}{\Omega_n - \omega - i\gamma_n} + \frac{\mu_{2,n} \mu_{1,n}}{\Omega_n + \omega + i\gamma_n} \right) \quad (7.4.1)$$

This time we used the following parameters:
 $\mu = [[3, -0.5], [1.2, 2.4]]$, $\Omega = [-3, 13]$, $\gamma = [0.7, 2.3]$, $N = 8$, $\varepsilon_0 = 1.4$, $h = -2.7$

Results are presented in the Figure 7.4.1. We can see a perfect match here!

Second-order model - results:

We have also used the same model as in 5.3 to describe the second-order susceptibility model:

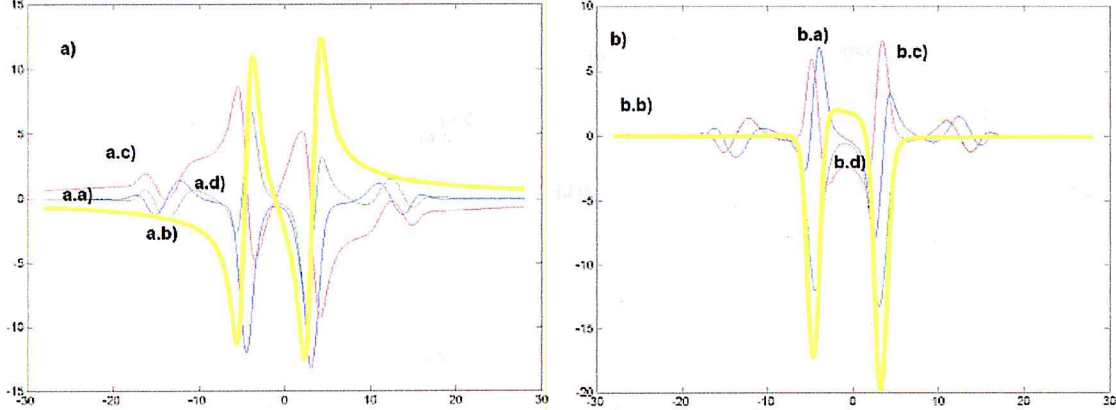


Figure 7.4.2: Results for the second-order quantum perturbative model for FHT Hilbert transform a.a) The plot of the real part of $\chi_{2,qp}(\omega)$ a.b) absolute error plot (a.d-plot minus a.c-plot) a.c) imaginary part of $\chi_{2,qp}(\omega)$ calculated analytically a.d) imaginary part of $\chi_{2,qp}(\omega)$ obtained with the Hilbert transform of a.a-plot, b.a) The plot of the imaginary part of $\chi_{2,qp}(\omega)$ b.b) absolute error plot (b.d-plot minus b.c-plot) b.c) real part of $\chi_{2,qp}(\omega)$ calculated analytically b.d) real part of $\chi_{2,qp}(\omega)$ obtained with the Hilbert transform of b.a-plot

$$\begin{aligned}
 \chi_{2,qp}(\omega_1, \omega_2) = & 2 N \varepsilon_0 h^2 \sum_{n=1}^2 \sum_{m=1}^2 \sum_{l=1}^2 \left(\frac{\mu_{l,n} \mu_{nm} \mu_{ml}}{(\Omega_{nl} - \omega_1 - \omega_2 - i\gamma_{nl})(\Omega_{ml} - \omega_1 - i\gamma_{ml})} + \right. \\
 & + \frac{\mu_{l,n} \mu_{nm} \mu_{ml}}{(\Omega_{nl} - \omega_1 - \omega_1 - i\gamma_{nl})(\Omega_{ml} - \omega_2 - i\gamma_{ml})} + \\
 & + \frac{\mu_{l,n} \mu_{nm} \mu_{ml}}{(\Omega_{mn} - \omega_1 - \omega_2 - i\gamma_{mn})(\Omega_{nl} + \omega_2 + i\gamma_{nl})} + \\
 & + \frac{\mu_{l,n} \mu_{nm} \mu_{ml}}{(\Omega_{mn} - \omega_1 - \omega_2 - i\gamma_{mn})(\Omega_{nl} + \omega_2 + i\gamma_{nl})} + \\
 & + \frac{\mu_{l,n} \mu_{nm} \mu_{ml}}{(\Omega_{nm} + \omega_1 + \omega_2 + i\gamma_{nm})(\Omega_{ml} - \omega_1 - i\gamma_{ml})} + \\
 & + \frac{\mu_{l,n} \mu_{nm} \mu_{ml}}{(\Omega_{nm} + \omega_1 + \omega_2 + i\gamma_{nm})(\Omega_{ml} - \omega_1 - i\gamma_{ml})} + \\
 & + \frac{\mu_{l,n} \mu_{nm} \mu_{ml}}{(\Omega_{ml} + \omega_1 + \omega_2 + i\gamma_{ml})(\Omega_{nl} + \omega_1 + i\gamma_{nl})} + \\
 & \left. + \frac{\mu_{l,n} \mu_{nm} \mu_{ml}}{(\Omega_{ml} + \omega_1 + \omega_2 + i\gamma_{ml})(\Omega_{nl} + \omega_2 + i\gamma_{nl})} \right), \quad (7.4.2)
 \end{aligned}$$

and we have used the following values of the constants:

$$\mu = \begin{vmatrix} 1 & 3 \\ -1 & -2 \end{vmatrix}, \quad \Omega = \begin{vmatrix} 3 & 16 \\ 4 & 12 \end{vmatrix}, \quad \gamma = \begin{vmatrix} 1 & 2 \\ -1 & 3 \end{vmatrix}, \quad N = 5, \quad \varepsilon_0 = 1, \quad h = -1$$

Results are presented in the Figure 7.4.2. As for the previous calculations, we can see the model could be invalid because of the raised errors reach up to 100%.

8 Hermite-Hilbert transform

8.1 Overview of the HHT

Hermite-Hilbert transform approach is based on the precalculation of already-known Hermite polynomials *Dasis* and Hermite base of orthogonal functions. The algorithm is based on the master thesis of Mathias Johansson [18].

Hermite polynomials and Hermite functions:

Hermite polynomial of an arbitrary n degree is defined as follows:

$$H_n(x) = \frac{(-1)^n e^{(x^2)} d^n e^{(-x^2)}}{dt^n} (-1)^n e^{x^2} \frac{d^n}{dx^n} e^{-x^2} \quad (8.1.1)$$

There is also an recursive equation for Hermite polynomials:

$$H_n(x) = 2x H_{n-1}(x) - 2(n-1) H_{n-2}(x) \quad (8.1.2a)$$

$$H_0(x) = 1 \quad H_1(x) = \dots \quad (8.1.2b)$$

Using the Hermite polynomial we would like to derive a set of orthogonal polynomials in L^2 . Therefore we introduce the weight function and the norm function:

$$w(x) = e^{-\frac{x^2}{2}} \quad (8.1.3a)$$

$$N_n(x) = \sqrt{2^n n! \sqrt{\pi}} \quad (8.1.3b)$$

If we multiply the n-th Hermite polynomial with the weight function $w(x)$ and divide it by the n-th norm function N_n we obtain a n-th orthogonal Hermite function:

$$\phi_n(x) = \frac{w(x) H_n(x)}{N_n(x)} = \frac{e^{-\frac{x^2}{2}} H_n(x)}{\sqrt{2^n n! \sqrt{\pi}}} \quad (8.1.4)$$

Based on the recursive equation in 8.1.2 we also obtain:

$$\phi_n(x) = \sqrt{\frac{2x \phi_{n-1}(x)}{n}} - (n-1) \sqrt{\frac{\phi_{n-2}(x)}{(n-1)n}} \quad (8.1.5a)$$

$$\phi_0(x) = \frac{e^{-\frac{x^2}{2}}}{\pi^{(\frac{1}{4})}} \quad (8.1.5b)$$

Hilbert transform of Hermite functions:

Johansson after polish mathematician Stefan L. Hahn [14] states that for any $f(x)$ and $\text{HILBERT}(f(x))$ belonging to L_1 we have:

$$\text{HILBERT}(x f(x)) = x \text{HILBERT}(F(x)) - \frac{1}{\pi} \int_{-\infty}^{\infty} f(\tau) d\tau \quad (8.1.6)$$

The proof of the Theorem stated in 8.1.6 is short:

$$\text{HILBERT}(x f(x)) = \frac{1}{\pi} \int_{-\infty}^{\infty} \frac{\tau f(\tau)}{x - \tau} d\tau = \frac{1}{\pi} \int_{-\infty}^{\infty} \frac{(x - s) f(x - s)}{s} ds, \quad (8.1.7)$$

$$\begin{aligned} \text{where } s &= x - \tau = \frac{1}{\pi} \int_{-\infty}^{\infty} \frac{x f(x - s)}{s} ds - \frac{1}{\pi} \int_{-\infty}^{\infty} f(x - s) ds = \\ &= x \text{HILBERT}(f(x)) - \frac{1}{\pi} \int_{-\infty}^{\infty} f(\tau) d\tau \end{aligned}$$

From both equations 8.1.6 and 8.1.5 we now obtain the important result:

$$\text{HILBERT}(\phi_n(x)) = \sqrt{\frac{2}{n}} \left(x \phi_{n-1}(x) - \frac{1}{\pi} \int_{-\infty}^{\infty} \phi_{n-1}(\eta) d\eta \right) - (n-1) \sqrt{\frac{1}{n(n-1)}} \phi_{n-2}(x) \quad (8.1.8a)$$

$$\text{HILBERT}(\phi_0(x)) = 2 \sqrt{2} \pi^{(\frac{1}{4})} \int_0^{\infty} e^{(-\frac{\omega^2}{2})} \sin(\omega x) d\omega \quad (8.1.8b)$$

Hilbert transform based on the Hermite functions:

Now we can derive the Hilbert transform of an arbitrary function. We start with expanding $f = f(x)$ into a series sum:

$$\begin{aligned} f(x) &= \sum_{n=0}^{\infty} a_n \phi_n(x) \quad (8.1.9a) \\ a_n &= \int_{-\infty}^{\infty} f(x) \phi_n(x) dx \quad (8.1.9b) \end{aligned}$$

For each function that has a limited series expansion at infinity we can provide an estimation used in further numerical algorithm:

$$f(x) \approx \sum_{n=0}^N a_n \phi_n(x) \quad (8.1.10a)$$

$$\text{HILBERT}(f(x)) \approx \sum_{n=0}^N a_n \text{HILBERT}(\phi_n(x)) \quad (8.1.10b)$$

Short description of the numerical algorithm:

Taking a look on the 8.1.10 we can see that the only difficulty is to calculate the a_n coefficients, while both the $\phi_n(x)$ and $\text{HILBERT}(\phi_n(x))$ can be precalculated once. The integral in 8.1.9 is now much easier because there is no singularity. The algorithm is given in Appendix A.5 and it consists of three main parts:

1. PRECALCULATION of the Hermite function coefficients with Maple Toolbox

MAIN LOOP:

2. ESTIMATION OF a_n COEFFICIENTS
3. CALCULATION OF THE HILBERT TRANSFORM (8.1.10b)

breaking
downlogics β_{in}

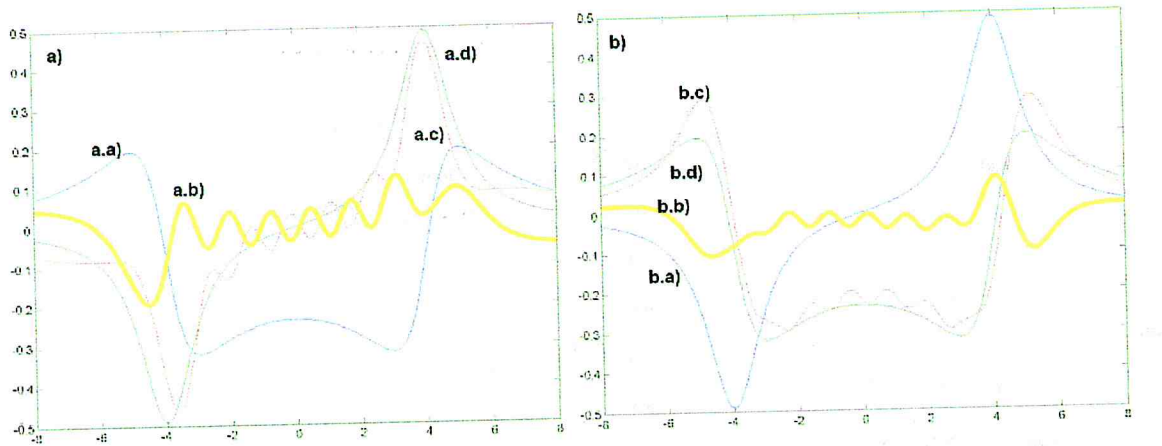


Figure 8.2.1: The Figure presents the results of the Hermite-Hilbert transform method applied to the simple linear model. Results are plotted together: a.a) The plot of the real part of $\chi(\omega)$ a.b) absolute error plot (c-plot minus d-plot) a.c) imaginary part of $\chi(\omega)$ obtained with the Hilbert transform of a-plot a.d) imaginary part of $\chi(\omega)$ calculated analytically. b.a) The plot of the imaginary part of $\chi(\omega)$ b.b) absolute error plot (c-plot minus d-plot) b.c) real part of $\chi(\omega)$ obtained with the Hilbert transform of a-plot b.d) real part of $\chi(\omega)$ calculated analytically.

8.2 HHT for simple linear model

In the Figure 8.2.1 we have presented the results obtained with the Hermite-Hilbert transform for the simple linear model defined in model 3.3.3. As we can see - the Hermite-Hilbert transform comes with poor accuracy, but we would like to put this method into examination with defined models.

8.3 HHT for simple nonlinear model

For the pump-probe and frequency mixing models we have used the same parameters as in chapter 5.3. The results obtained with the Hermite-Hilbert transform has been presented in Figures 8.3.1 and 8.3.2 respectively.

In these results we can draw two conclusions. The method based on the periodical polynomials as Hilbert polynomials will give us "zig-zag" like results. The other conclusion is that results obtained seems to be close, but much worst that those obtained with HCCI or FHT.

8.4 HHT for simple quantum-perturbative model

Linear model - results:

As in the Chapter 5.3, we have used the same model to describe the simple linear quantum-perturbative model:

$$\chi_{1,qp}(\omega) = \frac{N}{\varepsilon_0 h} \sum_{n=1}^2 \left(\frac{\mu_{1,n} \mu_{2,n}}{\Omega_n - \omega - i\gamma_n} + \frac{\mu_{2,n} \mu_{1,n}}{\Omega_n + \omega + i\gamma_n} \right) \quad (8.4.1)$$

This time we used the following parameters:

$$\mu = [[3, -0.5], [1.2, 2.4]], \Omega = [-3, 13], \gamma = [0.7, 2.3], N = 8, \varepsilon_0 = 1.4, h = -2.7$$

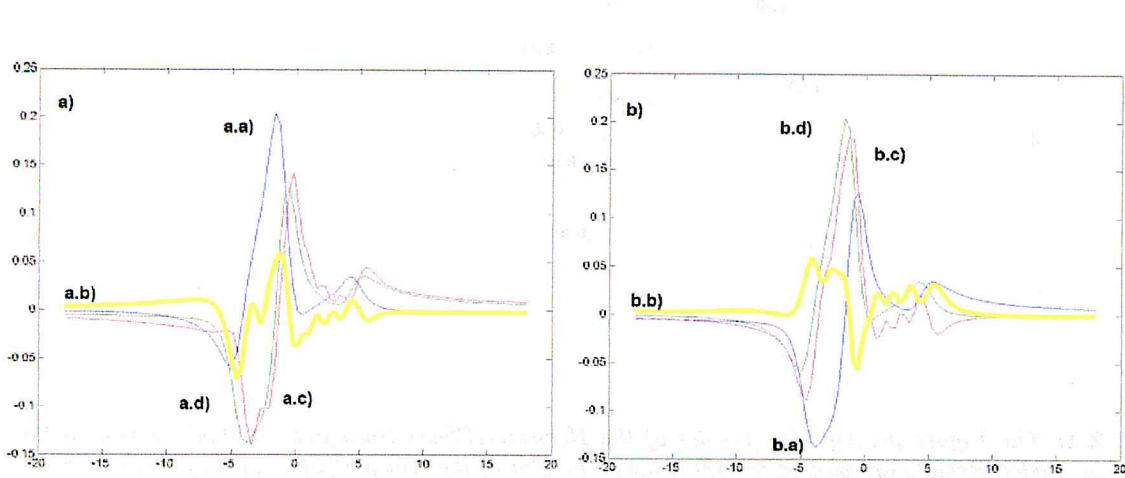


Figure 8.3.1: The Figure presents the results of the Hermite-Hilbert transform method applied to the pump-and-probe model. Results are plotted together: a.a) The plot of the real part of $\chi_{pp}(\omega)$ a.b) absolute error plot (a.d-plot minus a.c-plot) a.c) imaginary part of $\chi_{pp}(\omega)$ obtained with the Hermite-Hilbert transform of a.a-plot, a.d) imaginary part of $\chi_{pp}(\omega)$ calculated analytically b.a) The plot of the imaginary part of $\chi_{pp}(\omega)$ b.b) absolute error plot (b.d-plot minus b.c-plot) b.c) real part of $\chi_{pp}(\omega)$ obtained with the Hermite-Hilbert transform of b.a-plot b.d) real part of $\chi_{pp}(\omega)$ calculated analytically

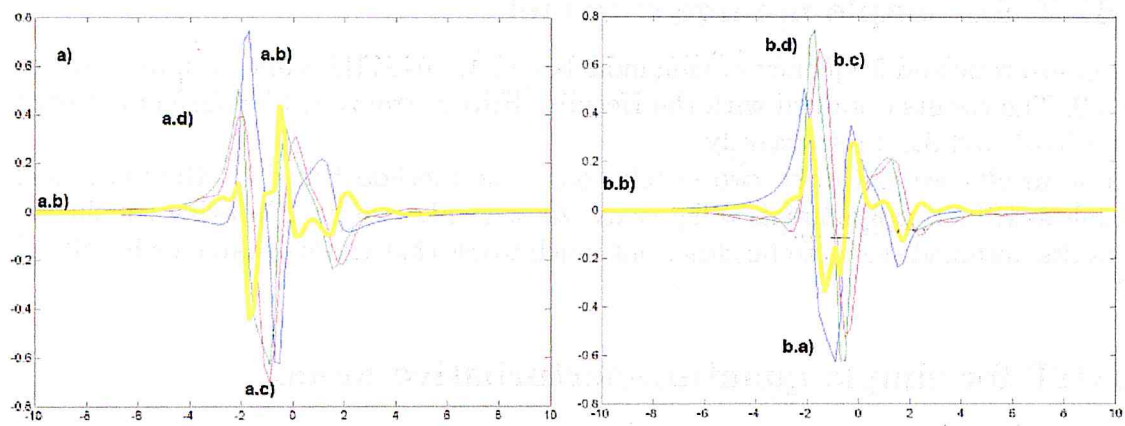


Figure 8.3.2: The Figure presents the results of the Hermite-Hilbert transform method applied to the frequency mixing model. Results are plotted together: a.a) The plot of the real part of $\chi_{mix}(\omega)$ a.b) absolute error plot (a.d-plot minus a.c-plot) a.c) imaginary part of $\chi_{mix}(\omega)$ obtained with the Hermite-Hilbert transform of a.a-plot, a.d) imaginary part of $\chi_{mix}(\omega)$ calculated analytically b.a) The plot of the imaginary part of $\chi_{mix}(\omega)$ b.b) absolute error plot (b.d-plot minus b.c-plot) b.c) real part of $\chi_{mix}(\omega)$ obtained with the Hermite-Hilbert transform of b.a-plot b.d) real part of $\chi_{mix}(\omega)$ calculated analytically

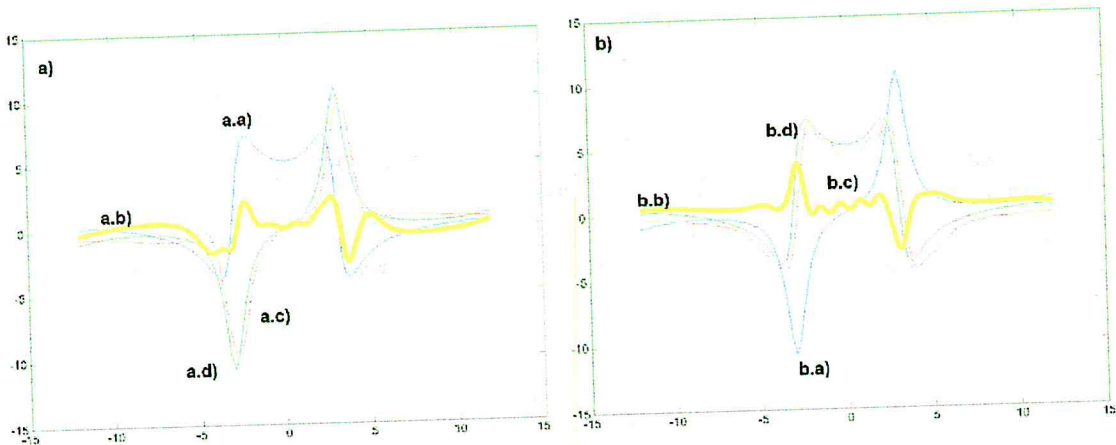


Figure 8.4.1: Results for the linear quantum perturbative model for Hermite-Hilbert transform a.a) The plot of the imaginary part of $\chi_{1,qp}(\omega)$ a.b) absolute error plot (d-plot minus c-plot) a.c) real part of $\chi_{1,qp}(\omega)$ obtained with the Hermite-Hilbert transform of a-plot a.d) real part of $\chi_{1,qp}(\omega)$ calculated analytically b.b) The plot of the real part of $\chi_{1,qp}(\omega)$ b.b) absolute error plot (d-plot minus c-plot) b.c) imaginary part of $\chi_{1,qp}(\omega)$ obtained with the Hermite-Hilbert transform of a-plot b.d) imaginary part of $\chi_{1,qp}(\omega)$ calculated analytically

Results are presented in the Figure 8.4.1.

Second-order model - results:

We have also used the same model as in 5.3 to describe the second-order susceptibility model:

$$\begin{aligned}
 & \text{V POPRAWIONO PÓŁTORAKI } \\
 \chi_{2,qp}(\omega_1, \omega_2) = & 2 N \varepsilon_0 h^2 \sum_{n=1}^2 \sum_{m=1}^2 \sum_{l=1}^2 \left(\frac{\mu_{l,n} \mu_{nm} \mu_{ml}}{(\Omega_{nl} - \omega_1 - \omega_2 - i\gamma_{nl})(\Omega_{ml} - \omega_1 - i\gamma_{ml})} + \right. \\
 & + \frac{\mu_{l,n} \mu_{nm} \mu_{ml}}{(\Omega_{nl} - \omega_1 - \omega_2 - i\gamma_{nl})(\Omega_{ml} - \omega_2 - i\gamma_{ml})} + \\
 & + \frac{\mu_{l,n} \mu_{nm} \mu_{ml}}{(\Omega_{mn} - \omega_1 - \omega_2 - i\gamma_{mn})(\Omega_{nl} + \omega_2 + i\gamma_{nl})} + \\
 & + \frac{\mu_{l,n} \mu_{nm} \mu_{ml}}{(\Omega_{mn} - \omega_1 - \omega_2 - i\gamma_{mn})(\Omega_{nl} + \omega_2 + i\gamma_{nl})} + \\
 & + \frac{\mu_{l,n} \mu_{nm} \mu_{ml}}{(\Omega_{nm} + \omega_1 + \omega_2 + i\gamma_{nm})(\Omega_{nl} - \omega_1 - i\gamma_{ml})} + \\
 & + \frac{\mu_{l,n} \mu_{nm} \mu_{ml}}{(\Omega_{nm} + \omega_1 + \omega_2 + i\gamma_{nm})(\Omega_{ml} - \omega_1 - i\gamma_{ml})} + \\
 & + \frac{\mu_{l,n} \mu_{nm} \mu_{ml}}{(\Omega_{ml} + \omega_1 + \omega_2 + i\gamma_{ml})(\Omega_{nl} + \omega_1 + i\gamma_{nl})} + \\
 & \left. + \frac{\mu_{l,n} \mu_{nm} \mu_{ml}}{(\Omega_{ml} + \omega_1 + \omega_2 + i\gamma_{ml})(\Omega_{nl} + \omega_2 + i\gamma_{nl})} \right), \quad (8.4.2)
 \end{aligned}$$

and we will be using the following constants values:

$$\mu = \begin{vmatrix} 1 & 3 \\ -1 & -2 \end{vmatrix}, \quad \Omega = \begin{vmatrix} 3 & 16 \\ 4 & 12 \end{vmatrix}, \quad \gamma = \begin{vmatrix} 1 & 2 \\ -1 & 3 \end{vmatrix}, \quad N = 5, \quad \varepsilon_0 = 1, \quad h = -1$$

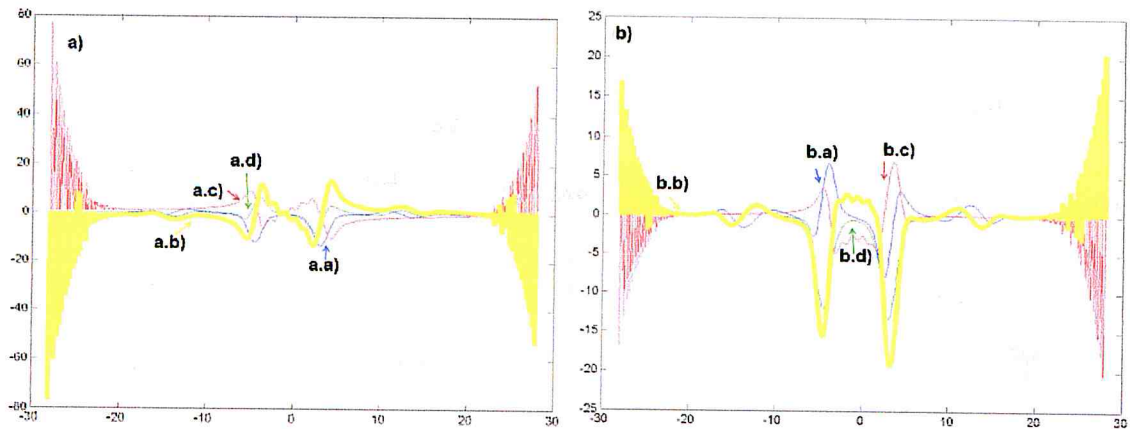


Figure 8.4.2: Results for the second-order quantum perturbative model for Hermite-Hilbert transform
 a) The plot of the real part of $\chi_{2,qp}(\omega)$ a.b) absolute error plot (a.d-plot minus a.c-plot) a.c)
 imaginary part of $\chi_{2,qp}(\omega)$ obtained with the Hermite-Hilbert transform of a.a-plot, a.d) imaginary part
 of $\chi_{2,qp}(\omega)$ calculated analytically b.a) The plot of the imaginary part of $\chi_{2,qp}(\omega)$ b.b) absolute error
 plot (b.d-plot minus b.c-plot) b.c) real part of $\chi_{2,qp}(\omega)$ obtained with the Hermite-Hilbert transform of
 b.a-plot b.d) real part of $\chi_{2,qp}(\omega)$ calculated analytically

Results are presented in the Figure 8.4.2. As for the previous calculations, we can see the model could be invalid because the occurring errors reach up to 100%.

We have checked the HHT method for various parameters, but none of them has given us better accuracy. We encourage the reader to carry out their own calculations with source code given in Appendix A.5.

9 Fourier-series

9.1 Overview of the Fourier-series based method

The concept of the Hilbert transform evaluation based on the Fourier series also comes from the master thesis by Mathias Johansson [18]. There is an important drawback in this approach - in general it should be applied to the periodic functions, but we will further assume they have a relatively long period. ✓

Fourier series:

Each periodical function can be decomposed into a infinite Fourier series. For a given periodic function f with a given period $2*P$, we will introduce the Fourier coefficients:

$$a_{f,n} = \int_{-P}^P f(x) \cos(nx) dx \quad (9.1.1a)$$

$$b_{f,n} = \int_{-P}^P f(x) \sin(nx) dx \quad (9.1.1b)$$

Not getting deeply into harmonic analysis - we will assume that a series of partial sums: *we know* *only*

$$S_{f,N}(x) = \frac{a_{f,0}}{2} + \left(\sum_{n=1}^N (a_{f,n} \cos(n x) + b_{f,n} \sin(n x)) \right) \quad (9.1.2)$$

for a function $f \in L_2(-P, P)$ converges at almost every point to the f , which can be written as:

poprawione

$$\text{if } S = \{t : \lim_{N \rightarrow \infty} S_{f,N}(t) \neq f(t)\} \text{ then } |S| \leq N_0 \quad (9.1.3)$$

Hilbert transform based on the Fourier series:

After Johansson [18] we state that for any given function f in $L_2(-P, P)$ we can calculate the Hilbert transform using the form of Fourier series for this function. All we need to do, is to make a swap in the 9.1.2 equation - the a_n coefficients should be swapped with b_n coefficients.

$$\begin{aligned} HILBERT(f(x)) &= \lim_{N \rightarrow \infty} \frac{a_{f,0}}{2} + \\ &+ \left(\sum_{n=1}^N (b_{f,n} \cos(n x) + a_{f,n} \sin(n x)) \right) \text{ [at alm. every point x]} \end{aligned} \quad (9.1.4)$$

Algorithm overview:

As mentioned before, we will prepare the algorithm as for the periodic function, but we will try to imply that the period is much longer than the area of interest. We would like to calculate the Hilbert transform for periodical and non-periodical function f . The first step is to calculate the properties of the input X interval, which is the region in which we are interested of both input function f values and the values of its Hilbert transform. The second step is to calculate the Fourier coefficients in a main loop. In the same loop we calculate the next partial sum values. The last step is to extract the inner interval from the extended interval, to omit the numerical errors near the interval edges.

The full source code of this algorithm, has been presented in the appendix A.6.

9.2 Fourier-series for simple linear model

In the Figure 9.2.1 we have presented the results obtained with the Fourier-Hilbert transform for the simple linear model defined in model 3.3.3. As we can see - the Fourier-Hilbert transform comes with poor accuracy, but we would like to put this method into examination with defined models.

9.3 Fourier-series for simple nonlinear model

For the pump-probe and frequency mixing models we have used the same parameters as in chapter 5.3. The results obtained with the Fourier-Hilbert transform has been presented in Figures 9.3.1 and 9.3.2 respectively.

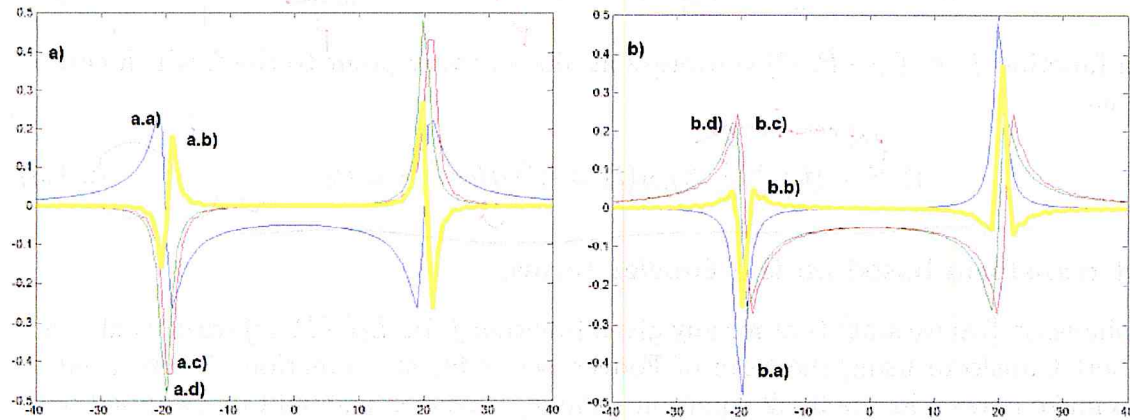


Figure 9.2.1: The Figure presents the results of the Hilbert transform based on the Fourier series method applied to the simple linear model. Results are plotted together: a.a) The plot of the real part of $\chi(\omega)$ a.b) absolute error plot (c-plot minus d-plot) a.c) imaginary part of $\chi(\omega)$ obtained with the Fourier-Hilbert transform of a-plot a.d) imaginary part of $\chi(\omega)$ calculated analytically. b.a) The plot of the imaginary part of $\chi(\omega)$ b.b) absolute error plot (c-plot minus d-plot) b.c) real part of $\chi(\omega)$ obtained with the Fourier-Hilbert transform of a-plot b.d) real part of $\chi(\omega)$ calculated analytically.

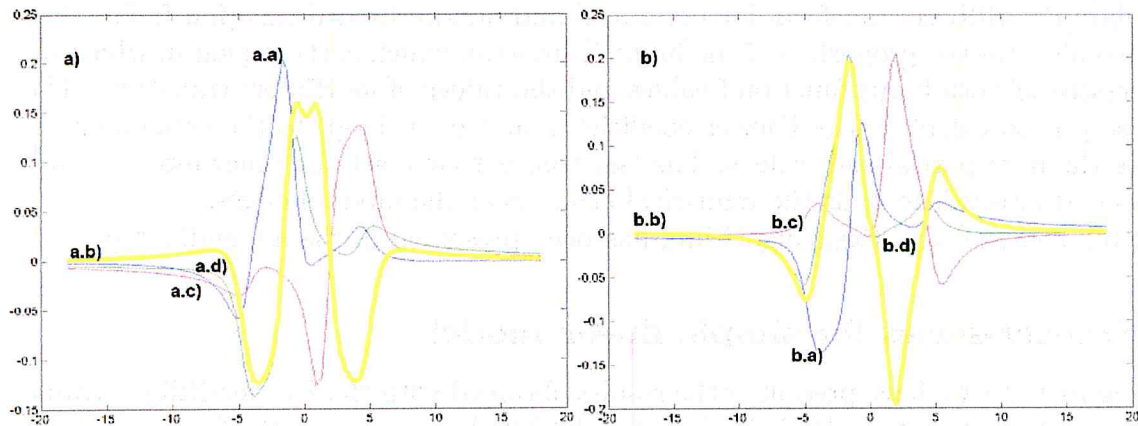


Figure 9.3.1: The Figure presents the results of the Hilbert transform based on the Fourier series method applied to the pump-and-probe model. Results are plotted together: a.a) The plot of the real part of $\chi_{pp}(\delta)$ a.b) absolute error plot (a.d-plot minus a.c-plot) a.c) imaginary part of $\chi_{pp}(\delta)$ obtained with the Fourier-Hilbert transform of a.a-plot, a.d) imaginary part of $\chi_{pp}(\delta)$ calculated analytically b.a) The plot of the imaginary part of $\chi_{pp}(\delta)$ b.b) absolute error plot (b.d-plot minus b.c-plot) b.c) real part of $\chi_{pp}(\delta)$ obtained with the Fourier-Hilbert transform of b.a-plot b.d) real part of $\chi_{pp}(\omega)$ calculated analytically

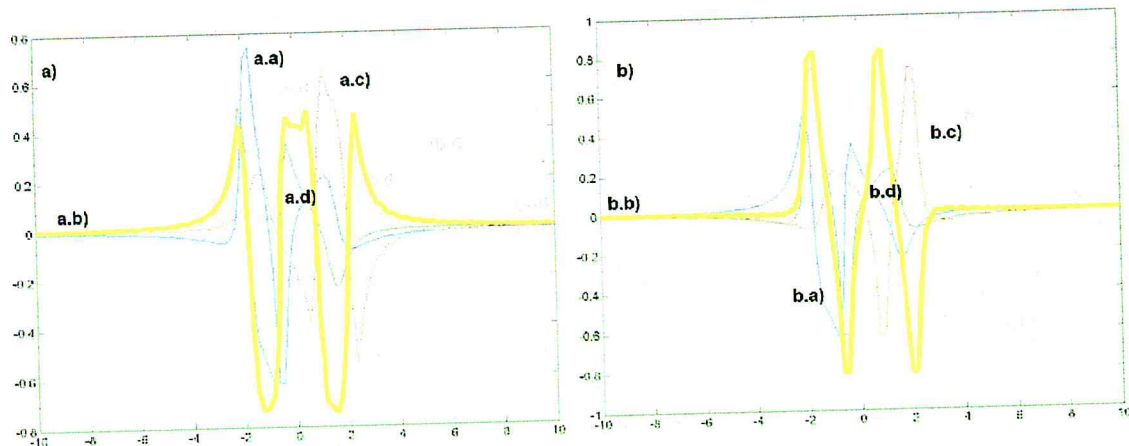


Figure 9.3.2: The Figure presents the results of the Hilbert transform based on the Fourier series method applied to the frequency mixing model. Results are plotted together: a.a) The plot of the real part of $\chi_{mix}(\omega)$ a.b) absolute error plot (a.d-plot minus a.c-plot) a.c) imaginary part of $\chi_{mix}(\omega)$ obtained with the Fourier-Hilbert transform of a.a-plot, a.d) imaginary part of $\chi_{mix}(\omega)$ calculated analytically b.a) The plot of the imaginary part of $\chi_{mix}(\omega)$ b.b) absolute error plot (b.d-plot minus b.c-plot) b.c) real part of $\chi_{mix}(\omega)$ obtained with the Fourier-Hilbert transform of b.a-plot b.d) real part of $\chi_{mix}(\omega)$ calculated analytically

In these results we can draw two conclusions. The method based on the periodical polynomials as Fourier series will give us “zig-zag” like results. The other conclusion is that results obtained seems to be close, but much worst that those obtained with HCCI or FHT.

9.4 Fourier-series for simple quantum-perturbative model

Linear model - results:

As in the Chapter 5.3, we have used the same model to describe the simple linear quantum-perturbative model:

$$\chi_{1,qp}(\omega) = \frac{N}{\varepsilon_0 h} \sum_{n=1}^2 \left(\frac{\mu_{1,n} \mu_{2,n}}{\Omega_n - \omega - i\gamma_n} + \frac{\mu_{2,n} \mu_{1,n}}{\Omega_n + \omega + i\gamma_n} \right) \quad (9.4.1)$$

This time we used the following parameters:

$$\mu = [[3, -0.5], [1.2, 2.4]], \Omega = [-3, 13], \gamma = [0.7, 2.3], N = 8, \varepsilon_0 = 1.4, h = -2.7.$$

Results are presented in the Figure 9.4.1.

Second-order model - results:

We have also used the same model as in 5.3 to describe the second-order susceptibility model:

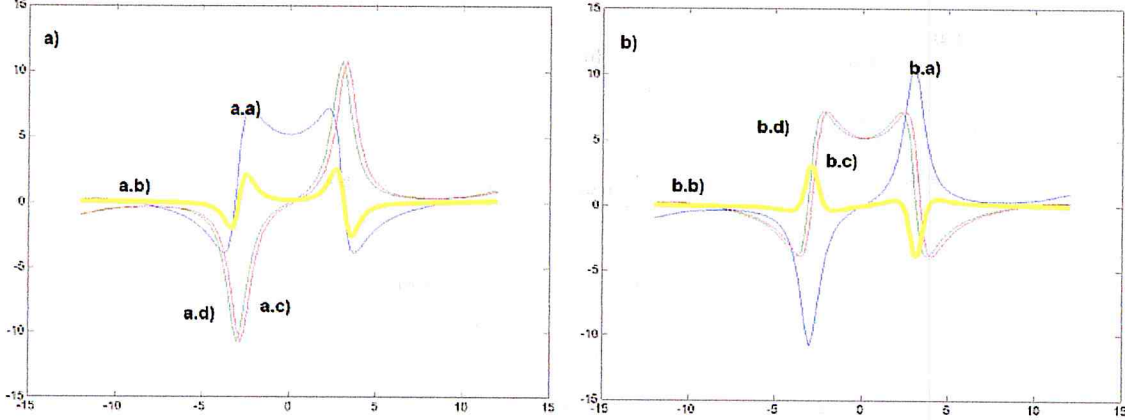


Figure 9.4.1: Results for the linear quantum perturbative model for Fourier-Hilbert transform *a.a)* The plot of the imaginary part of $\chi_{1,qp}(\omega)$ *a.b)* absolute error plot (d-plot minus c-plot) *a.c)* real part of $\chi_{1,qp}(\omega)$ obtained with the Fourier-Hilbert transform of *a*-plot *a.d)* real part of $\chi_{1,qp}(\omega)$ calculated analytically *b.b)* The plot of the real part of $\chi_{1,qp}(\omega)$ *b.b)* absolute error plot (d-plot minus c-plot) *b.c)* imaginary part of $\chi_{1,qp}(\omega)$ obtained with the Fourier-Hilbert transform of *a*-plot *b.d)* imaginary part of $\chi_{1,qp}(\omega)$ calculated analytically

$$\begin{aligned} \chi_{2,qp}(\omega_1, \omega_2) = & 2 N \varepsilon_0 h^2 \sum_{n=1}^2 \sum_{m=1}^2 \sum_{l=1}^2 \left(\frac{\mu_{l,n} \mu_{nm} \mu_{ml}}{(\Omega_{nl} - \omega_1 - \omega_2 - i\gamma_{nl})(\Omega_{ml} - \omega_1 - i\gamma_{ml})} + \right. \\ & + \frac{\mu_{l,n} \mu_{nm} \mu_{ml}}{(\Omega_{nl} - \omega_1 - \omega_2 - i\gamma_{nl})(\Omega_{ml} - \omega_2 - i\gamma_{ml})} + \\ & + \frac{\mu_{l,n} \mu_{nm} \mu_{ml}}{(\Omega_{mn} - \omega_1 - \omega_2 - i\gamma_{mn})(\Omega_{nl} + \omega_2 + i\gamma_{nl})} + \\ & + \frac{\mu_{l,n} \mu_{nm} \mu_{ml}}{(\Omega_{mn} - \omega_1 - \omega_2 - i\gamma_{mn})(\Omega_{nl} + \omega_2 + i\gamma_{nl})} + \\ & + \frac{\mu_{l,n} \mu_{nm} \mu_{ml}}{(\Omega_{nm} + \omega_1 + \omega_2 + i\gamma_{nm})(\Omega_{ml} - \omega_1 - i\gamma_{ml})} + \\ & + \frac{\mu_{l,n} \mu_{nm} \mu_{ml}}{(\Omega_{nm} + \omega_1 + \omega_2 + i\gamma_{nm})(\Omega_{ml} - \omega_1 - i\gamma_{ml})} + \\ & + \frac{\mu_{l,n} \mu_{nm} \mu_{ml}}{(\Omega_{ml} + \omega_1 + \omega_2 + i\gamma_{ml})(\Omega_{nl} + \omega_1 + i\gamma_{nl})} + \\ & \left. + \frac{\mu_{l,n} \mu_{nm} \mu_{ml}}{(\Omega_{ml} + \omega_1 + \omega_2 + i\gamma_{ml})(\Omega_{nl} + \omega_2 + i\gamma_{nl})} \right), \quad (9.4.2) \end{aligned}$$

and we will be using the following constants values: $\mu = \begin{vmatrix} 1 & 3 \\ -1 & -2 \end{vmatrix}$, $\Omega = \begin{vmatrix} 3 & 16 \\ 4 & 12 \end{vmatrix}$, $\gamma = \begin{vmatrix} 1 & 2 \\ -1 & 3 \end{vmatrix}$, $N = 5$, $\varepsilon_0 = 1$, $h = -1$.

Results are presented in the Figure 9.4.2. We can see, that the first model could be valid, while the second model seems to be invalid for consecutively for all Hilbert transform implementations.

We have checked the Fourier-Hilbert method for various parameters, but none of them has gave us better accuracy. We encourage the reader to carry out their own calculations.

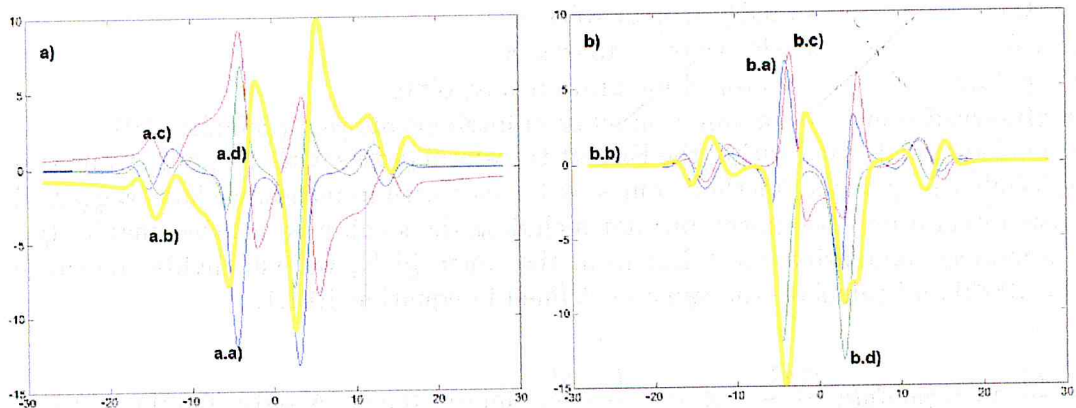


Figure 9.4.2: Results for the second-order quantum perturbative model for Fourier-Hilbert transform a.a) The plot of the real part of $\chi_{2,qp}(\omega)$ a.b) absolute error plot (a.d-plot minus a.c-plot) a.c) imaginary part of $\chi_{2,qp}(\omega)$ obtained with the Fourier-Hilbert transform of a.a-plot, a.d) imaginary part of $\chi_{2,qp}(\omega)$ calculated analytically b.a) The plot of the imaginary part of $\chi_{2,qp}(\omega)$ b.b) absolute error plot (b.d-plot minus b.c-plot) b.c) real part of $\chi_{2,qp}(\omega)$ obtained with the Fourier-Hilbert transform of b.a-plot b.d) real part of $\chi_{2,qp}(\omega)$ calculated analytically

with source code given in Appendix A.6.

10 MATLAB ® out-of-the-box functions

10.1 Overview of the MATLAB ® interior functions

Why not take into consideration the already built-in numerical methods from MATLAB? We compare the results obtained with:

- quadgk() - adaptive Gauss-Kronrod quadrature;
- hilbert() - fast Hilbert transform based on both FFT and IFFT.

Adaptive Gauss-Kronrod quadrature - theory:

The source code of the adaptive Gauss-Kronrod quadrature has been published in the popular Fortran 77 numerical integration QUADPACK library and has been also translated into the MATLAB core language. It is also based on the "quadva" routine described by Lawrence F. Shampine in [36]. The fundamental idea of this numerical integration algorithm is the nested quadrature rule - the more accurate quadrature approximation is calculated from the less accurate one. The algorithm is adaptive and the error estimation is based on the (G-K7,15) pair of the quadrature rules - less and more accurate - the 7-point Gauss rule and the 15-point Kronrod rule with a share nodes. For more information about the theory beneath this algorithm - please read D. Calvetti et al [7] or the chapter 5.5 from the book by David Kahaner [19].

Adaptive Gauss-Kronrod quadrature - short tutorial:

We have used the MATLAB ®R2009b. It comes with built-in quadgk function with four parameters:

~~GK(f, a, b)~~

'AbsTol'

- absolute error tolerance

'RelTol'

- relative error tolerance

'Waypoints'

- vector of integration waypoints

'MaxIntervalCount'

- maximum number of intervals allowed (default: 650)

The defined models used within the Hilbert transform comes with one, but strong singularity. While the quadgk() method comes with copes with infinities, we have suggested to split the integral into two parts, but not including the small area nearby singularity.

If the models singularity c is taken from the range $[a, b]$, we will divide the range $|b - a|$ by 10000 and calculate the value as defined in equation 10.1.1.

$$\int_{-\infty}^{\infty} \frac{f(x)}{x-c} dx \approx \text{quadgk}\left(\frac{f(x)}{x-c}, -\infty, c - \frac{|b-a|}{10000}, \text{'RelTol', 0.001, 'AbsTol', 0.001}\right) \quad (10.1.1)$$

$$+ \text{quadgk}\left(\frac{f(x)}{x-c}, c + \frac{|b-a|}{10000}, +\infty, \text{'RelTol', 0.001, 'AbsTol', 0.001}\right)$$

Fast Hilbert transform routine - theory:

The discrete Hilbert transform (DHT) is given by definition after [20] - for a given n-length X vector:

$$\text{DHT}(X_k) = \frac{1}{n} \left(\sum_{s=0}^{n-1} X_s (1 - (-1)^{(k-s)}) \cot\left(\frac{\pi(k-s)}{n}\right) \right) \quad (10.1.2)$$

The other definition by [7] uses the convolution:

$$\text{DHT}(X_k) = X[] * h[] = \sum_{s=0}^{n-1} h_{k-s} X_s \quad (10.1.3a)$$

$$h_k = \frac{1}{n} \left(\cot\left(\frac{\pi k}{n}\right) - \frac{\cos(\pi k)}{\sin(\frac{\pi k}{n})} \right) \quad (10.1.3b)$$

The important issue is that the DHT is closely related to the discrete Fourier transform (DFT). For a given n-length X vector in order to evaluate the DHT(X) we can hire the DFT routine. To start, we must remember that in the continuous case:

$$\text{FOURIER}(\text{HILBERT}(X_k)) = \left(-i \operatorname{sgn}\left(\frac{n}{2} - k\right) \operatorname{sgn}(k)\right) \text{FOURIER}(X_k), \quad (10.1.4)$$

where we remember that:

$$-i \operatorname{sgn}\left(\frac{n}{2} - k\right) \operatorname{sgn}(k) = \text{FOURIER}\left(\frac{1}{\pi k}\right). \quad (10.1.5)$$

Therefore, in the discrete case we find the similar equation to 10.1.4 relating the DHT and DFT:

$$\text{DFT}(\text{DHT}(X_k)) = \left(-i \operatorname{sgn}\left(\frac{n}{2} - k\right) \operatorname{sgn}(k)\right) \text{DFT}(X_k) \quad (10.1.6)$$

From the 10.1.6 we can see, that it is quite easy to operate within the Fourier/frequency domain - because the quite complicate convolution is transformed to a simple

65

$$\int \frac{f(x)}{x-c} dx = \int f(\cos\theta + x) d\theta$$

$\int \frac{f(x)}{x-c} dx$
 c + cos
 c - cos

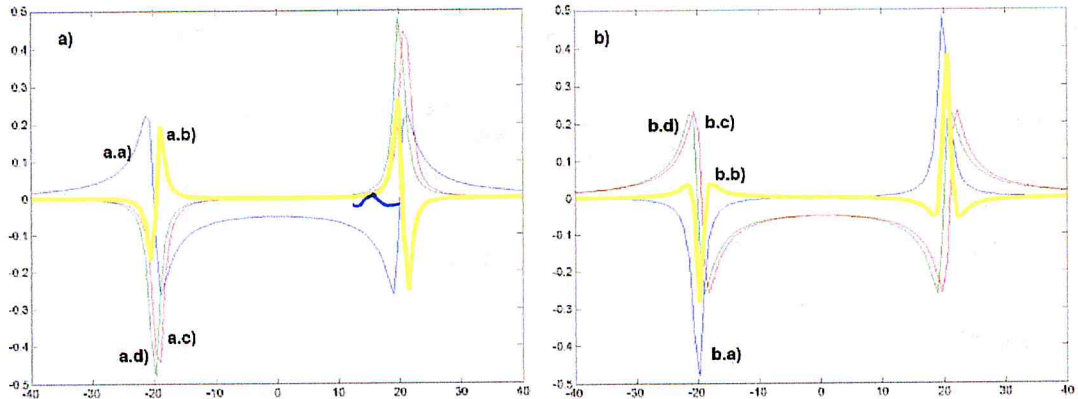


Figure 10.2.1: The Figure presents the results of the `quadgk()` method applied to the simple linear model. Results are plotted together: a.a) The plot of the real part of $\chi(\omega)$ a.b) absolute error plot (c-plot minus d-plot) a.c) imaginary part of $\chi(\omega)$ obtained with the `quadgk()`-Hilbert transform of a-plot a.d) imaginary part of $\chi(\omega)$ calculated analytically. b.a) The plot of the imaginary part of $\chi(\omega)$ b.b) absolute error plot (c-plot minus d-plot) b.c) real part of $\chi(\omega)$ obtained with the `quadgk()`-Hilbert transform of a-plot b.d) real part of $\chi(\omega)$ calculated analytically.

algebraic operations. Also - if we have the quick algorithm to perform both the DFT and inverse-DFT - for example with the fast Fourier transform (FFT) and the inverse fast Fourier transform (IFFT) - the DHT operation will be calculated as follows:

$$\text{DHT}(X_k) = \text{IDFT}\left((-i) \operatorname{sgn}\left(\frac{n}{2} - k\right) \operatorname{sgn}(k) \text{DFT}(X_k)\right) \quad (10.1.7)$$

Fast Hilbert transform routine - short tutorial:

While the hired DFT and IDFT routines are evaluated in complex domain, for a given input n-length X vector we have that:

$$\underline{\text{hilbert}}(X) \Rightarrow X + i \text{DHT}(X) \quad (10.1.8)$$

In order to obtain the final result we need to take the imaginary part of the MATLAB `hilbert()` function output. The other important issue is that the *MATLAB® hilbert()* function has one optional parameter called N - to computer the N-point Hilbert transform. If the input vector X is too short, it will be padded with zeros, otherwise it will be truncated.

10.2 MIF for simple linear model

In two Figures 10.2.1 and 10.2.2 we have gathered the results obtained with the MATLAB `quadgk()` and `hilbert()` functions based Hilbert transforms for the simple linear model defined in model (3.3.3). For each method we can see a acceptable accuracy.

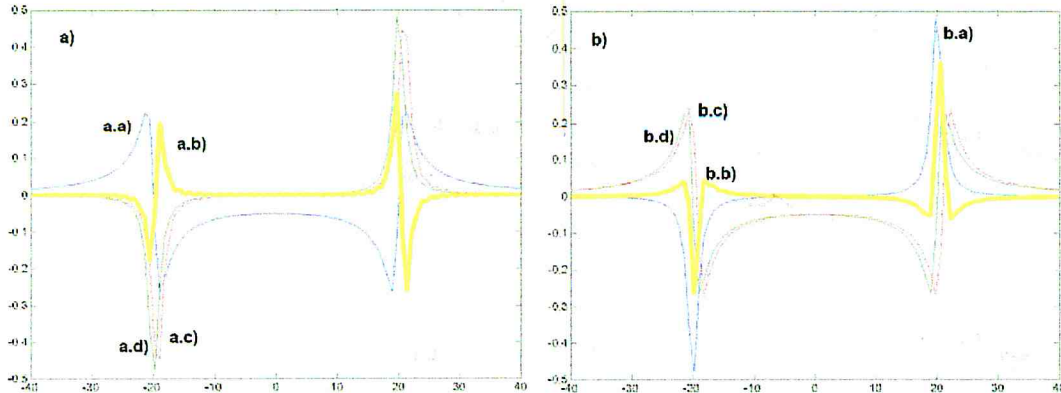


Figure 10.2.2: The Figure presents the results of the `hilbert()` method applied to the simple linear model. Results are plotted together: a.a) The plot of the real part of $\chi(\omega)$ a.b) absolute error plot (c-plot minus d-plot) a.c) imaginary part of $\chi(\omega)$ obtained with the `hilbert()` transform of a-plot a.d) imaginary part of $\chi(\omega)$ calculated analytically. b.a) The plot of the imaginary part of $\chi(\omega)$ b.b) absolute error plot (c-plot minus d-plot) b.c) real part of $\chi(\omega)$ obtained with the `hilbert()` transform of a-plot b.d) real part of $\chi(\omega)$ calculated analytically.

10.3 MIF for simple nonlinear model

In the next four Figures: 10.3.1, 10.3.2, 10.3.3 and 10.3.4 we have gathered the results obtained with the MATLAB® `quadgk()` and `hilbert()` functions based Hilbert transforms for the pump-probe and frequency mixing models with the same parameters as in chapter 5.3.

For each method we can once again see the acceptable accuracy for each method, but we can also observe, that each method comes with noticeable error.

10.4 MIF for simple quantum-perturbative model

We have also put the determined methods onto test with quantum-perturbative models taken from chapter 5.3.

Linear model - results:

In the Figures: 10.4.1 and 10.4.2 we have gathered the results obtained with the MATLAB `quadgk()` and `hilbert()` functions based Hilbert transforms for the linear quantum-perturbative model taken with the same parameters as in chapter 5.3.

We observe quite acceptable results for the investigated model, for both methods applied.

Second-order model - results:

In the Figures: 10.4.3 and 10.4.4 we have gathered the results obtained with the MATLAB `quadgk()` and `hilbert()` functions based Hilbert transforms for the second-order quantum-perturbative model taken with the same parameters as in chapter 5.3.

We observe a huge error as in all previously chapters for the investigated model, for both methods applied.

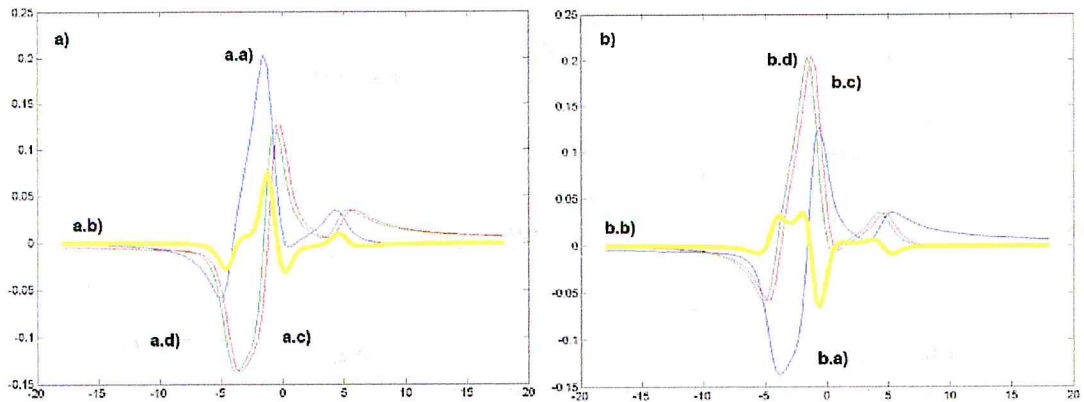


Figure 10.3.1: Results for the pump-probe model using the `quadgk()` Hilbert transform *a.a)* The plot of the real part of $\chi_{pp}(\omega)$ *a.b)* absolute error plot (*a.d*-plot minus *a.c*-plot) *a.c)* imaginary part of $\chi_{pp}(\omega)$ obtained with the `quadgk()` Hilbert transform of *a.a*-plot, *a.d)* imaginary part of $\chi_{pp}(\omega)$ calculated analytically *b.a)* The plot of the imaginary part of $\chi_{pp}(\omega)$ *b.b)* absolute error plot (*b.d*-plot minus *b.c*-plot) *b.c)* real part of $\chi_{pp}(\omega)$ obtained with the `quadgk()` Hilbert transform of *b.a*-plot *b.d)* real part of $\chi_{pp}(\omega)$ calculated analytically

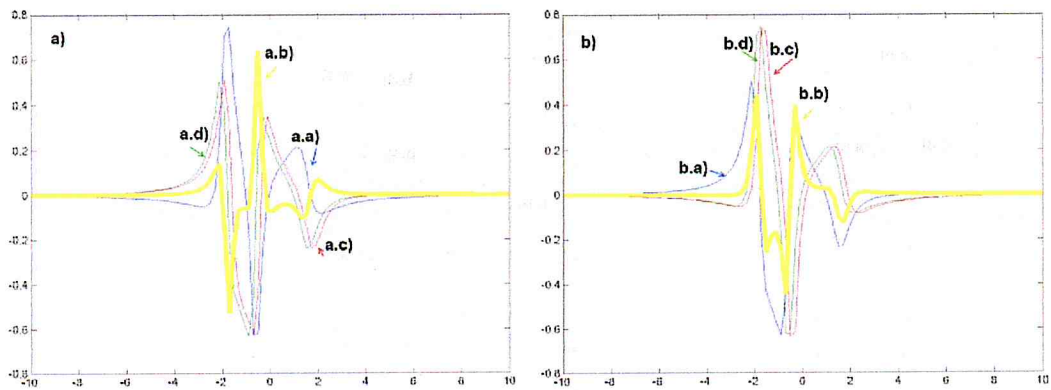


Figure 10.3.2: Results for the frequency model using the `quadgk()` Hilbert transform *a.a)* The plot of the real part of $\chi_{pp}(\omega)$ *a.b)* absolute error plot (*a.d*-plot minus *a.c*-plot) *a.c)* imaginary part of $\chi_{pp}(\omega)$ obtained with the `quadgk()` Hilbert transform of *a.a*-plot, *a.d)* imaginary part of $\chi_{pp}(\omega)$ calculated analytically *b.a)* The plot of the imaginary part of $\chi_{pp}(\omega)$ *b.b)* absolute error plot (*b.d*-plot minus *b.c*-plot) *b.c)* real part of $\chi_{pp}(\omega)$ obtained with the `quadgk()` Hilbert transform of *b.a*-plot *b.d)* real part of $\chi_{pp}(\omega)$ calculated analytically

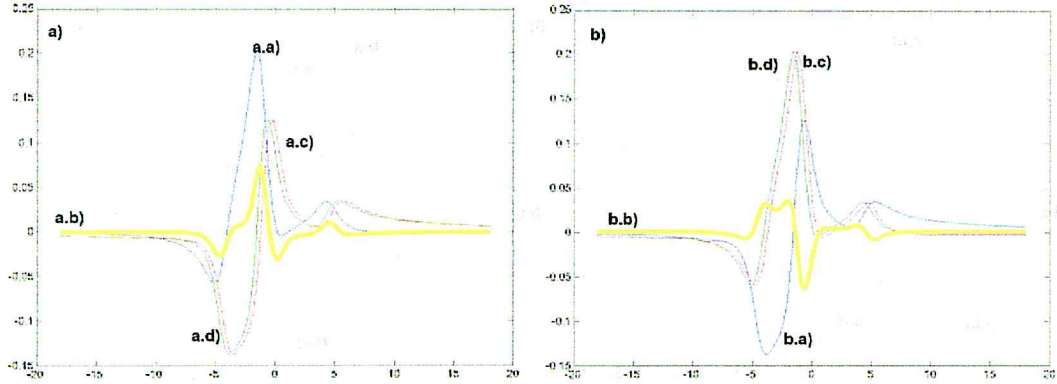


Figure 10.3.3: Results for the pump-probe model using the `hilbert()` transform a.a) The plot of the real part of $\chi_{mix}(\omega)$ a.b) absolute error plot (a.d-plot minus a.c-plot) a.c) imaginary part of $\chi_{mix}(\omega)$ obtained with the `hilbert()` transform of a.a-plot, a.d) imaginary part of $\chi_{mix}(\omega)$ calculated analytically b.a) The plot of the imaginary part of $\chi_{mix}(\omega)$ b.b) absolute error plot (b.d-plot minus b.c-plot) b.c) real part of $\chi_{mix}(\omega)$ obtained with the `hilbert()` transform of b.a-plot b.d) real part of $\chi_{mix}(\omega)$ calculated analytically

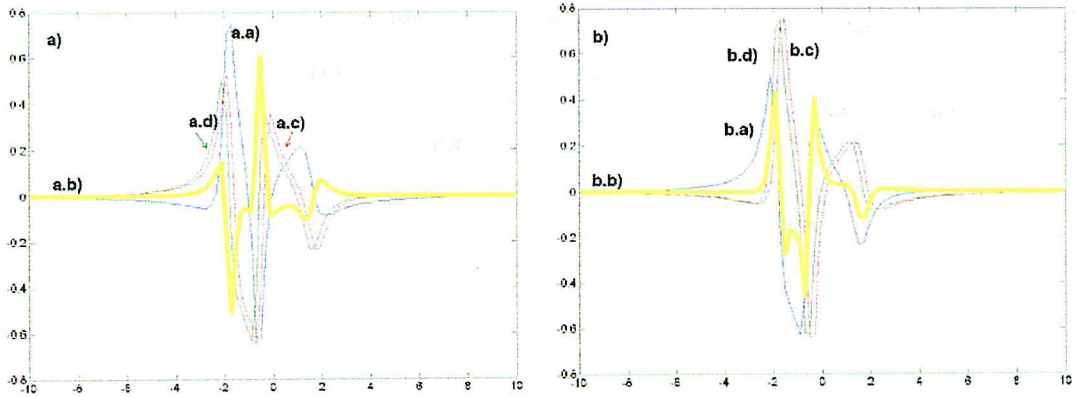


Figure 10.3.4: Results for the frequency mixing model using the `hilbert()` transform a.a) The plot of the real part of $\chi_{pp}(\omega)$ a.b) absolute error plot (a.d-plot minus a.c-plot) a.c) imaginary part of $\chi_{pp}(\omega)$ obtained with the `hilbert()` transform of a.a-plot, a.d) imaginary part of $\chi_{pp}(\omega)$ calculated analytically b.a) The plot of the imaginary part of $\chi_{pp}(\omega)$ b.b) absolute error plot (b.d-plot minus b.c-plot) b.c) real part of $\chi_{pp}(\omega)$ obtained with the `hilbert()` transform of b.a-plot b.d) real part of $\chi_{pp}(\omega)$ calculated analytically

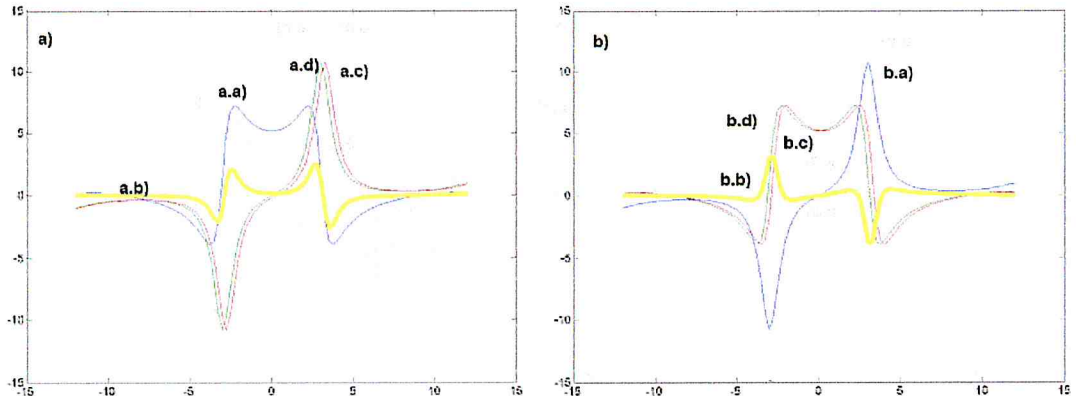


Figure 10.4.1: Results for the linear quantum perturbative model for `quadgk()` Hilbert transform a.a) The plot of the imaginary part of $\chi_{1,qp}(\omega)$ a.b) absolute error plot (d-plot minus c-plot) a.c) real part of $\chi_{1,qp}(\omega)$ obtained with the `quadgk()` Hilbert transform of a-plot a.d) real part of $\chi_{1,qp}(\omega)$ calculated analytically b.b) The plot of the real part of $\chi_{1,qp}(\omega)$ b.b) absolute error plot (d-plot minus c-plot) b.c) imaginary part of $\chi_{1,qp}(\omega)$ obtained with the `quadgk()` Hilbert transform of a-plot b.d) imaginary part of $\chi_{1,qp}(\omega)$ calculated analytically

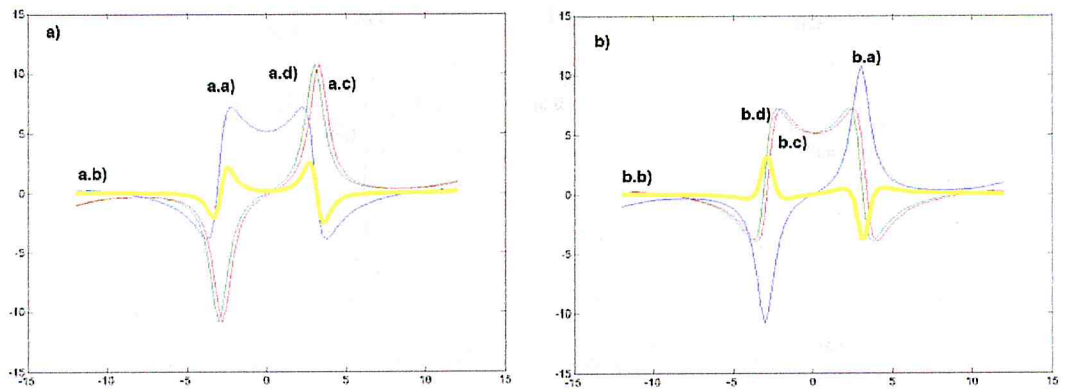


Figure 10.4.2: Results for the linear quantum perturbative model for `hilbert()` transform a.a) The plot of the imaginary part of $\chi_{1,qp}(\omega)$ a.b) absolute error plot (d-plot minus c-plot) a.c) real part of $\chi_{1,qp}(\omega)$ obtained with the `hilbert()` transform of a-plot a.d) real part of $\chi_{1,qp}(\omega)$ calculated analytically b.b) The plot of the real part of $\chi_{1,qp}(\omega)$ b.b) absolute error plot (d-plot minus c-plot) b.c) imaginary part of $\chi_{1,qp}(\delta)$ obtained with the `hilbert()` transform of a-plot b.d) imaginary part of $\chi_{1,qp}(\delta)$ calculated analytically

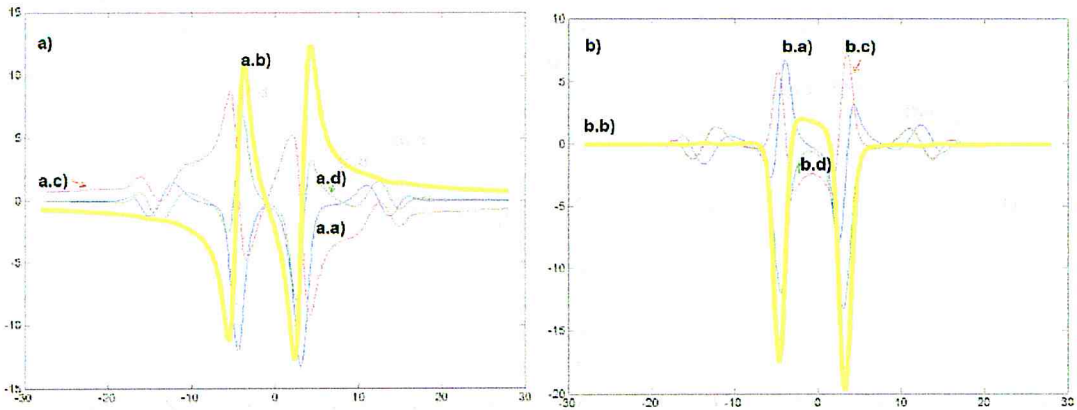


Figure 10.4.3: Results for the second-order quantum perturbative model for `quadgk()` Hilbert transform
 a.a) The plot of the imaginary part of $\chi_{1,qp}(\omega)$ a.b) absolute error plot (d-plot minus c-plot) a.c) real part of $\chi_{1,qp}(\omega)$ obtained with the `quadgk()` Hilbert transform of a-plot a.d) real part of $\chi_{1,qp}(\omega)$ calculated analytically
 b.b) The plot of the real part of $\chi_{1,qp}(\omega)$ b.b) absolute error plot (d-plot minus c-plot) b.c) imaginary part of $\chi_{1,qp}(\omega)$ obtained with the `quadgk()` Hilbert transform of a-plot b.d) imaginary part of $\chi_{1,qp}(\omega)$ calculated analytically

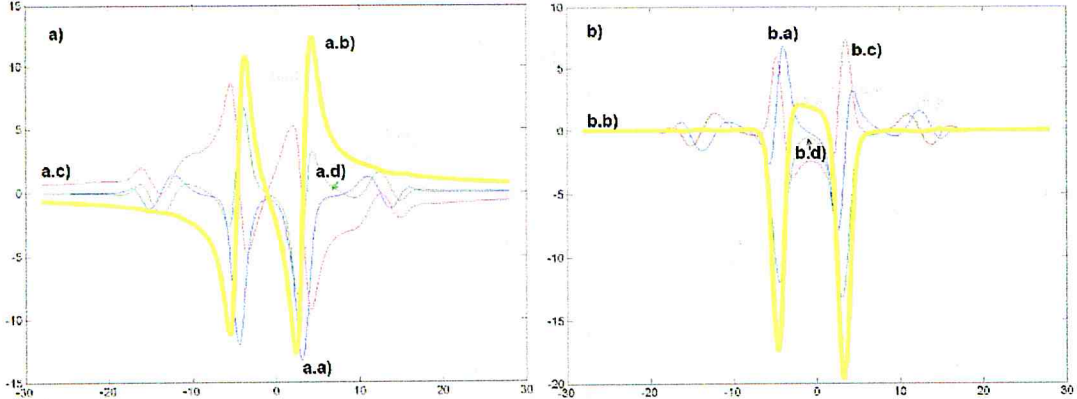


Figure 10.4.4: Results for the second-order quantum perturbative model for `hilbert()` transform a.a) The plot of the imaginary part of $\chi_{1,qp}(\omega)$ a.b) absolute error plot (d-plot minus c-plot) a.c) real part of $\chi_{1,qp}(\omega)$ obtained with the `hilbert()` transform of a-plot a.d) real part of $\chi_{1,qp}(\omega)$ calculated analytically
 b.b) The plot of the real part of $\chi_{1,qp}(\omega)$ b.b) absolute error plot (d-plot minus c-plot) b.c) imaginary part of $\chi_{1,qp}(\omega)$ obtained with the `hilbert()` transform of a-plot b.d) imaginary part of $\chi_{1,qp}(\omega)$ calculated analytically

Table 2: Time comparison

method name	time used for all 5 models
HTRAN	1.8095s
Newton-Cotes	122.1465s
Clenshaw-Curtis	776.7389s
Hartley	9.5106s
Hermite	6.7423s
Fourier	443.3777s
quadgk()	325.0274s
hilbert()	0.46756s

← prelicyjne ver

Table 3: Accuracy comparison

method name	linear	pump-probe	freq. mix.	quant. linear	quant. 2 nd -order
HTRAN	7	5	5	5	2
Newton-Cotes	7	4	4	3	2
Clenshaw-Curtis	9	9	8	7	3
Hartley	8	8	7	6	3
Hermite	6	5	3	3	0
Fourier	6	5	3	3	0
quadgk()	7	7	6	5	3
hilbert()	7	7	6	5	3

11 General comparison of numerical methods used

11.1 Time comparison conclusions:

Until now we have not mention how much time does it take for each of investigated methods to calculate desired results. In the Table 2 we have showed how much time does it take to perform the calculations for all 5 investigated models.

As we can see - the investigated methods come with important timing differences. When preparing experiment data analysis we should choose the appropriate method reasonably.

11.2 Accuracy comparison conclusions:

We have prepare the subjective summary of the accuracy obtained with investigated methods with the zero (bad accuracy) to ten (good accuracy). It is presented in the table 3.

11.3 Application comparison conclusions:

There are two main types of methods - those, which base on the full-vector calculation (like HTRAN, Hartley-Hilbert transform, hilbert()) and those, which require calculation for each point (Newton-Cotes, Clenshaw-Curtis, Hermite-Hilbert, Fourier-Hilbert, quadgk()). The first group comes with relative acceptable accuracy, but still not negligible one.

On the other side we can use the Clenshaw-Curtis based implementation of the Hilbert transform - which has showed as the method with the best accuracy from all investigated methods.

When we would analyze data that has been collected in one dimension - it would be a good idea to hire the accurate, but slow Clenshaw-Curtis Hilbert transform implementation. But we should also prepare a good method for two-dimensional calculation and for such case we should use the fast methods like Hartley-Hilbert transform or built-in MATLAB `@hilbert()` method.

But what is a good information - all methods can be used in the model analysis and validation process.

12 Conclusion

We have presented a valid implementation of several different approaches to calculate the improper and singular integral used in the Hilbert transform. During the implementation and the literature research we have confirmed, that despite of talking about the complicate Kramers-Kronig relations, we can hire the simpler Hilbert transform.

12.1 Model conclusion

During work on this thesis we have found at least one invalid model - such as second-order quantum-perturbative model. For none of implemented method this model has shown any acceptable type of accuracy. There were more such models, not taken into scope - but with described tools - an experienced research will be able to validate model with the Hilbert transform relations.

The one hypothetical proposal of explanation the failure of the second-order quantum-perturbative model is that this model as the only investigate one - depends on two input frequencies. The theory of multi-dimensional Hilbert transform states, that one point depends on the whole multi-dimensional spectra. What we have done here - was the false assumption - that for such a model we can simple strike on dimension out. This assumption proved to be false.

The multi-dimensional Hilbert transform is beyond the scope of this work and requires the better knowledge of implementation the multi-dimensional singular quadratures.

12.2 Numerical conclusion

1. We have presented several methods and the comparison of their accuracy, convergency and speed. Which method is the best and why? This set of tools should be treated as a numerical tool box - the choice is always depends on the user's choice. 2. The speed-leading methods are based on the full-vector calculations. There are a good candidates for the multi-dimensional hilbert transform integration.

12.3 Z-scan technique conclusion

In our opinion the data collected from the Z-scan experiment can be put into test with all prepared methods. We should also remember, that the phenomena occurring during

this experiment - due to strong energy - shows the complicated nonlinearity, so the multi-dimensional Hilbert transform methods may be required.

12.4 General conclusion

The aim of this work was to:

- Development of numerical methods of the Hilbert transform. It succeeded and the methods are available altogether with their source code and the testing routines. Users can choose among a wide range of methods with described parameters.
- Validation of models given in literature. This succeeded only for the most popular models. There is a wide range of models given in literature for which the Hilbert transform rule simple does not work.
- Carrying out the calculations on multi-dimensional models. It failed. It turned out that such calculations require much more complex numerical methods.

Other conclusions:

1. This thesis is only an introduction into the important, but still not well described, hardly-investigated interdisciplinary problem concerning the investigation of light and matter interaction in area of nonlinear optics.

2. This topic should be continued as the cooperation between various disciplines is the key role to solve many questions stated by nowadays nonlinear optics scientists - so the strong mathematical, numerical, chemical and quantum-mechanical background skills are together required, one person is unable to have it all, so a team should be created (here in Wrocław).

"A major challenge for researchers working in a multidisciplinary area is the need to learn relevant concepts outside their expertise. This may require searching through a vast amount of literature, often leading to frustrations of not being able to extract pertinent information quickly." - P. Prasad [32]

3. We can find many papers in area of Kramers-Kronig for nonlinear optics, but in my opinion - in case of nonlinear optics many of them are false and not properly argued, with wrong or improper mathematical assumptions, numerical errors and sometimes even tendential optimism and non-scepticism, which - especially in area of modern physics - is incomprehensible.

4. We are all in a long run for a Nobel prize :) It's a huge motivation :)

12.5 Further questions and research direction

What should be the continuation of this work?

- The theory which is linking the Hilbert transform with nonlinear optical models should be more deeply investigated. How can the influence of subsequent photons shooting the investigated sample be described with only one equation?
- Many literature models should be validated and a list of both valid and invalid models should be publicated.

- The valid and proper tools for multi-dimensional Hilbert transform should be prepared

Other open questions: 1. Should we always use the Fourier transform when translating between the time-domain and the frequency domain?

2. As the linear model in optical research is quite well described, we need to prepare tools for the nonlinear calculations, which involve operating on the two-dimensional data sets. There are algorithms like 2D-FFT, 2D-FHT, maybe there also can be an algorithm for 2D-hilbert transform.

3. How to efficiently perform calculations for higher dimensional data (f.e. third-order or fifth-order nonlinear phenomena)?

4. We need to make a further research on the topic of the harmonic analysis and Fourier analysis and its application to the spectral analysis.

13 Acknowledgements

I would mostly thank Professor Marek Samoć for introducing me into the magical world of the nonlinear optics. In my opinion there is an important niche between this scientific domain and the numerical analysis, there are also many questions that I am asking now myself (beyond the scope of this thesis) and I would like to find answers in the future.

I would give my acknowledgements for many people from the Wrocław University of Technology, especially:

Katarzyna Matczyszyn, PhD

for inspirations to work between two or more scientific domains and to work for others,

Dr. Marcin Nyk, PhD

for a very good mood each time I needed it and for introducing me into the world of real chemical experiments

Chris Corkey, PhD

for Your great smile, great mood and inspiration to travel

All OM-IN-NANO Great TEAM!

I would like to thank You all guys for your hard work and for the great time and experience not only in the real and hard research, but also in a top-science. You are coping with guys! Thank also You for all Your answers to all my (usually simple) questions.

Great honours should be also given for the members of the University of Wrocław. I would like to give my acknowledgements for:

Rafał Keller, PhD

for supervising me through the hard area of quadratures with singularities

Professor Stanisław Lewanowicz

for the review of this work, useful comments and inspiration to think outside the cubicle

Grzegorz Karch, PhD

for introducing me into the world of advanced differential and integral calculus